NASA CONTRACTOR REPORT 166366

NASA-CR-166366
19820021375

FOR ~~~~~~

Pioneer 10/11 Data Analysis of the
Magnetic Field Experiment

NOT TO BE TAKEN ~~~~~~~~~~~

Douglas E. Jones

Brigham Young University

NASA

NF02625

N82-29251

Pioneer 10/11 Data Analysis of the
Magnetic Field Experiment

Douglas E. Jones

Brigham Young University
Provo, Utah

Summary

This final report covers work conducted by Brigham Young University personnel in support of the Pioneer missions to Jupiter (10, 11) and Saturn (11) as well as the reduction, analysis and interpretation of magnetic field data obtained by the vector helium magnetometer (VHM) on the Pioneer 10 and 11 spacecraft. Initially, our efforts concentrated primarily on the interplanetary data, and those aspects of the data of relevance to obtaining a better understanding of the interaction of the magnetized solar wind with the terrestrial magnetic field. However, after we participated in the encounters of Jupiter and Saturn, the emphasis of our research was directed primarily to an analysis of the planetary data. In particular, it soon became clear that there was a need for modelling of the various candidate magnetospheric currents suggested by the data.

Over the period of this contract (7/1/73-12/31/81) we have supported the launch, cruise, and encouter phases of the Pioneer 10 and 11 missions, published 16 papers, presented 15 papers, and had 19 abstracts of papers published. A listing of the papers and abstracts published is given in the "List of Publications." In the next sections we summarize the work conducted in various research areas conducted under this contract. Included are results not published as yet, but which we plan to publish.

The August 1972 Solar Flare Event

During August, 1972, considerable flaring activity occured on the sun, which in turn produced significant modification of the solar wind medium as measured at a number of spacecraft, including Pioneer 10. In addition, significant terrestrial effects were observed. We worked closely with E. J. Smith of JPL during this period and conducted some additional analysis of our own that were based upon the hypothesis that flare producing regions rather than specific flares are the causal source of interplanetary and terrestrial events. Although we did not complete the analysis of this event in terms of the flare region hypothesis because of pressures resulting from the encounter of Jupiter, nevertheless there were a number of characteristics of the data (both field and energetic particle) that were consistent with this latter hypothesis. That is, effects were seen in space and at earth when the flare producing region (region on the surface of the sun having a history of flaring) was at the proper angular relationship with respect to the earth considering the finite travel time at nominal solar wind velocities, and it was not necessary to hypothesize that a flare erupted on the unseen portion of the sun. The results of a standard analysis and interpretation of these data has been published ,although we are planning to develop and present our alternate hypothesis (L. Davis et al., 1973; E. Smith et al., 1977).

The Measurement of Weak Magnetic Fields in Space

During the period of this research we studied a proposed method to measure weak magnetic fields using two magnetometers in a coorrelative mode purported to reduce the resultant magnetometer sensor noise to an insignificant amount. We found that the basic premise of the paper was in serious error, and that in fact the method proposed would not work. The results of this brief study were published (Jones, et al., 1974).

Interior Source Magnetic Field Modelling: Jupiter

Our initial modelling efforts as applied to the Pioneer 10 data consisted of the utilization of a function minimization approach to finding the field sources that best fit the data obtained within about 7 RJ (D. E. Jones and J. G. Melville, 1974; E. J. Smith, et al., 1974). When a single offset dipole was used as the interior source of the field, we found that as the radial range of the data used in the fitting was increased, equatorial projection of the end of the vector describing the offset of the equivalent dipole would tend to describe a circle. A more complicated field source configuration consisting of two dipoles plus a uniform field was then used, the latter being the dominant term of an external ring current. The use of two dipoles was based upon the results of ground based radio astronomy interferometer mapping and polarization measurements which suggested the existence of a magnetic anomally near the surface of the planet near a System III longitude of 200°. For simplicity, we chose to represent this anomaly in our studies as a magnetic dipole. The other dipole was assumed to be the primary source of the planet's magnetic field.

A function minimization (FMFD) algorithm was developed which internally varied the location, orientation and strength of the two dipoles, as well as the parameters of the uniform field, until a best fit was obtained to the data in a least squares sense. Using the Pioneer 10 data, it was found that the resulting residuals were smaller than those obtained using the conventional linear, or spherical harmonic, approach. We found that a plot of the residuals versus radial distance exhibited high values at about the orbital distance of Io. The Voyager later confirmed that the flux tube of Io contained currents, and suggested the presence of a plasma torus at this orbital distance. The second dipole was found to be located close to the equator in the hemisphere, close to the longitude of the radio astronomy polarization anomaly, and reasonably close to the surface.

A similar type of analysis was performed using the Pioneer 11 data with results that were consistent with that obtained from Pioneer 10. The second dipole was located in the same longitudinal quadrant as that of Pioneer 10 and reasonably close to the surface, but in the southern hemisphere. We are not sure what effect the existence of tail and frontside cross sheet current fields will have on the location of the second dipole as determined from the Pioneer 10 and 11 data, but it is clear that the use of such an analysis approach has merit, particularly if proper allowance for the fields from these other currents results

in more consistent characteristics for the two interior dipole sources as derived from the two spacecraft data sets. An extension of this work, which included the Pioneer 11 results as well as a SHA analysis of data from both spacecraft, used a different weighting scheme, and derived more information concerning the ring current, was written up as an undergraduate thesis for the honors program by R. Steven Turley and has been included as Appendix A of this report.

Modelling the Jovian Magnetosphere

During the period of this contract we have studied the Jovian magnetosphere using two basic methods. The first involved the use of Euler potentials, a method which results in mathematical expressions that permit easy tracing of field lines. Some degree of success was achieved in obtaining functions describing the field which provided reasonable fits to the data, and which were useful when extrapolated a small distance beyond the region of fitting. As the result of a cooperative program with the energetic particle experiment team at the University of Iowa, it was found that the outbound Pioneer 10 was periodically located on open field lines, this occurring while at fairly low magnetic latitudes (Goertz, et al., 1976). This result was obtained by comparing the spacecraft location in magnetic coordinates with the energetic particle measurements. The existence of an open/closed field line demarcation at such a low magnetic latitude (approximately 20°) was rather startling at the time, but this may be consistent with the general topology of the magnetic field in the sunward magnetosphere as inferred from the outbound Pioneer 11 magnetic field measurements, which suggests that it is quite different from that of earth.

We attempted to use an Euler potential approach in the study of the magnetosphere beyond $\pm 20^\circ$ magnetic latitude, with little success. We found that the unphysical magnetic fields and currents predicted at high latitudes by the functions that were tried far outweighed the advantages of these functions (Jones and Melville, 1975). In addition, the deformations of the current disc evident in the data could not be accomodated in a tractable manner with such a function. We tried several coordinate systems, with little success.

In order to facilitate a current disc clearly displaying twisting and bending, we subsequently developed an algorithm for the magnetic field of a double layer of circular rings of current which allowed the tilt and longitude of the axis of each ring making up the disc to be functions of the ring radius. In addition, we desired a model for the currents which could be used to extrapolate beyond the region of fitting with more reliability than the Euler function method. Excellent agreement was obtained between model predictions and the data, with parametric expressions being developed for the manner in which the current disc was deformed, particularly using Pioneer 10 outbound data. It was found that the disc needed to be twisted about the spin axis, and bent such as to approach parallelism with the rotational equator. An additional deformation of the current disc in the form of a small ridge or hump was required in order

- 4 -

for the spacecraft to periodically penetrate the bent disc.
Figures 1-6 compare the current discs required to fit the Pioneer
10 outbound data (Figs. 1-3; twisted and bent, with spiralling
ridge) and the Voyager data (Figs. 4-6; twisted and bent only).
The Pioneer 11 inbound data also suggested that some degree of
bending improved the fits. The other data sets clearly required
additional tail field and required discs displaying markedly
different characteristics as to the amount and distribution of
current, as well as the amount of tilting required (Melville et
al., 1975; Jones et al., 1975; Jones and Melville, 1975; Jones et
al., 1976a,b; 1980; 1981; Jones and Thomas, 1981). An extreme
case in point is the fact that in order to fit the strong current
dip observed outbound at about 8 R_J by Pioneer 11, a tilt of over
35° is required, whereas the inbound Pioneer 11 data require a
thinner disc having a tilt of 11.2^o. A study was also conducted
to determine the radial current distribution required to produce
a fit to the azimuthal field from both the outbound Pioneer 10
and 11 data.
       When the characteristics of the ring currents for the
various data segments were compared, both the rho and phi field
components displayed a local time dependence. As an alternate to
local time dependent disc and radial currents, it was suggested
the possibiliy of an azimuthally symmetric disc current plus a
sheet of dusk to dawn current, the latter being the equatorial
portion of a tail-like current configuration extending into the
frontside magnetosphere (Jones, et al., 1981; Jones and Thomas,
1981). Such a configuration produces the observed maximum in the
rho and phi components near the dawn line, and the decrease in
these components near the noon meridian. A preliminary study of
the fields of such a current configuration has resulted in fits
to the data which are better than those obtained in terms of a
local time dependent disc current and tail/magnetopause currents
(Jones and Thomas, 1981).

Magnetic Field and Energetic Particle Flux Studies
       Several analysis efforts were conducted in an attempt to
better understand the relationship between the energetic particle
flux and the magnetic field. Using the model disc current which
best fit the Pioneer 10 outbound data, we traced out field lines
to determine the L values corresponding to important times
related to observed characteristics of the energetic particles.
As a result, a joint paper was presented outlining the L
dependence of the energetic particles in Jupiter's magnetosphere
(Jones and Mihalov, 1978). This study was based upon a model
disc current system fitting the outbound Pioneer 10 data, where
good fits were obtained without tail and magnetopause currents
(these currents produce primarily positive and negative z fields,
respectively, and they are apparently of the same magnitude near
the dawn meridian). Hence, the magnetosphere was not terminated,
and a reanalysis of the particle data using L values derived from
a terminated magnetosphere, or using model paramters derived from
fitting other data segments should modify the results reported
previously.
       We have also explored the locations of minimum field regions

that result when a magnetosphere is terminated by the solar
wind. A model fitting the Pioneer 10 data has been combined with
a system of currents on the surface of a sphere to derive a
terminated magnetosphere. The resulting magnetopause was blunt,
and consistent with the derived shape of the magnetopause using
minimum variance techniques. The field minima produced by the
termination were shifted away from the magnetic equator,
resulting in two surfaces oriented at a relatively large angle
relative to the magnetic equator. When the Pioneer 11 outbound
trajectory was superimposed on the field line disgram derived
from the model, it was found that the occurances of the field
minima were reasonably consistent with the observed occurances of
the energetic particle maxima (Jones, 1979). Other analyses of
the Pioneer 11 outbound field data suggest several other possible
explanations for the anomalously high flux counts at such a high
latitude. One considers the possibility that the localized tilt
of the current disc near the noon meridian was much greater ($>$
30°) (Jones et al., 1975; Jones et al., 1976a,b) while the other
considers the possibility that the magnetospheric cleft is at a
much lower latitude, the latter providing a region for the
energetic particles to escape from the planet (Jones and Thomas,
1931).

Satellite-Magnetosphere Interaction Studies at Saturn.

When the 24 hour interval of data spanning the closest
approach of Titan's orbit by Pioneer 11 was studied, it was found
that there were three periods in which the level of magnetic
variability was enhanced: One of these occured spanning several
hours before to one or two hours after closest approach to Titan,
when the spacecraft was about 145 R_t (Titan radii) ahead of the
satellite in the direction of orbital motion. The
characteristics of these turbulent regions were studied and it
was concluded that the Titan interval displayed a number of
characteristics that are consistent with what would be expected
should the spacecraft penetrate the satellites magnetic wake.
Evidence for penetration of a shock so far "downstream" was weak,
and marginal at best, but there was a field minimum almost
precisely at closest approach to the extended tail axis, and the
characteristics of the magnetic turbulence of the Titan interval
appeared to differ from those of the other two. As a result of
this analysis, we suggested that the magnetic wake of Titan may
have been detected (Jones et al., 1979; Jones et al., 1980).

Preliminary studies of the magnetic data near the time of
the energetic particle decreases attributed to the new satellite
1979 S-2 suggested the possible existence of low Alfven mach
number fans associated with the interaction of a satellite with
corotating plasma. However, a closer inspection of the manner in
which the various field components varied during this interval
suggested this not to be the case. It was later determined that
this was a data anomaly that resulted from the use of a despin
function that did not properly take into account acceleration of
the spacecraft at Saturn and the nonlinear characteristics of an
improper despin function timing anomaly in the data produced the
false result (Jones et al., 1979a,b).

List of Publications and Papers Presented *

1. E. J. Smith, L.Davis, Jr., D. E. Jones, P. J. Coleman, Jr., C. P. Sonett, P. Dyal, and D. S. Colburn, "The Distant Interplanetary Magnetic Field: Pioneer 10," Trans. Amer. Geophys. Union, 54, 438 (1973) (Abstract of paper presented at A.G.U. Meeting, April 1973).

2. L. Davis, Jr. E. J. Smith, D. E. Jones, P. J. Coleman, Jr., P. Dyal, and C.P. Sonett, "Pioneer 10 Observations of Interplanetary Shocks from the August 1972 Flares," Trans. Amer. Geophys. Union, 54, 438 (1973) (Abstract of paper presented at A.G.U. Meeting, April 1973).

3. E. J. Smith, L. Davis, Jr., D. E. Jones, P. J. Coleman, Jr., D. S. Colburn, P. Dyal, and C. P. Sonett, "Measurement of the Distant Interplanetary Magnetic Field on Pioneers 10 and 11," Trans. Amer. Geophys. Union, 54, 1197 (1973). (Abstract of paper presented at A.G.U. Meeting, December 1973).

4. E. J. Smith, L. Davis, Jr., D. E. Jones, D. S. Colburn, P. J. Coleman, Jr., P. Dyal, and C. P. Sonett, "The Magnetic Field of Jupiter and its Interaction with the Solar Wind," Science, 183, 305 (1974).

5. D. E. Jones, E. J. Smith, and J. G. Melville, "Discussion of the Paper: 'A note on Signal Enhancement for Dual Magnetometer Systems' by N. F. Ness," J. Geophys. Res., 79, 2927 (1974).

6. E. J. Smith, L. Davis, Jr., D. E. Jones, P. J. Coleman, Jr., D. S. Colburn, P. Dyal, and C. P. Sonett, "The Magnetic Field of Jupiter and Its Interaction with the Solar Wind," Trans. Amer. Geophys. Union, 55, 413 (1974) (Abstract of paper presented at A.G.U. Meeting April, 1974).

7. D.E. Jones, E.J. Smith, L. Davis, Jr., D.S. Colburn, P.J. Coleman, Jr., P. Dyal, and C.P. Sonett, "Pioneer 10 Measurements of Jupiters Magnetic Field," Proc. Utah Acad. Sci. Arts and Letters, 51, 153 (1974).

8. D. E. Jones and J. G. Melville, "A Study of Single and Dual Dipole Magnetic Field Models for Jupiter: Pioneer 10," Proc. Utah Acad. Sci., Arts and Letters, 51, 161 (1974).

9. E. J. Smith, L. Davis, Jr., D. E. Jones, P. J. Coleman, Jr., D. S. Colburn, P. Dyal, C. P. Sonett, and A. M. A. Frandsen, "The Planetary Magnetic Field and Magnetosphere of Jupiter: Pioneer 10," J.G.R., 79, 3501 (1974).

10. D. E. Jones, E. J. Smith and L. Davis, Jr., "Measurement of the magnetic field of Jupiter by Pioneers 10 and 11". (Paper presented at the Gordon Conference on Space Plasma Physics, Franklin Pierce College, Rindge, N.H., June 9 -13, 1975.

11. J. G. Melville, M. L. Blake, and D. E. Jones, "Modeling Jupiter's intense disc current," (Paper presented at the Fall Meeting of the Utah Academy of Sciences, Arts and Letters, November, 1975.)

12. D. E. Jones and J. G. Melville, "Preliminary model studies of the magnetosphere of Jupiter: Pioneer 10," Proc. of the Utah Acad. of Sci., Arts and Letters, 52, 14, 1975. (Abstract of paper presents at the Spring Meeting of the Utah Academy of Sciences, Arts and Letters, April, 1975.)

13. E. J. Smith, L. Davis, Jr., D. E. Jones, P. J. Coleman, Jr., D. S. Colburn, P. Dyal, and C. P. Sonett, "Jupiters Magnetic Field, Magnetosphere, and Interaction with the Solar Wind," Science, 188, 451 (1975).

14. L. Davis, Jr., E. J. Smith, and D. E. Jones, "The Magnetic Field of Jupiter," Trans. Amer. Geophys. Union, 56, 1041 (1975) (Abstract of paper presented at A.G.U. Meeting, December 1975).

15. E. J. Smith, L. Davis, Jr., D. E. Jones, P. J. Coleman, Jr., D. S. Colburn, and C. P. Sonett, "The Planetary Magnetic Field and Magnetosphere of Jupiter: Pioneer 11 Vector Helium Magnetometer," Bull. of Am. Astron. Soc., 7, 379 (1975). (Abstract of paper presented at Planetary Sciences Div. of A.A.S.).

16. C. K. Goertz, D. E. Jones, B. A. Randall, E. J. Smith, and M. F. Thomsen, "Evidence for Open Field Lines on Jupiter's Magnetosphere," J. Geophys. Res., 81, 3393 (1976).

17. E. J. Smith, L. Davis, Jr., and D. E. Jones, "Jupiter's Magnetic Field and Magnetosphere," Chapter in Jupiter; Studies of the Interior, Atmosphere, Magnetosphere and Satellites, University of Arizona Press, Tucson, Arizona, (1976) ed. by T. Gehrels.

18. J. G. Melville, II, (Comment made after "Jupiters magnetic field and magnetosphere," by Smith et al., pp. 826,7) in Jupiter; Studies of the Interior, Atmosphere, Magnetosphere and Satellites, University of Arizona Press, Tucson, Arizona, (1976) ed. by T. Gehrels.

19. D. E. Jones and J. G. Melville II, "Modeling Jupiter's magnetospheric current disc: Pioneer 10 and 11," Proc. Utah Acad. Sci., Arts, and Letters, 53, 61, 1976. (Abstract of paper presented at Fall Meeting of the Utah Academy of Sciences, Arts and Letters, November, 1976.)

20. D. E. Jones, E. J. Smith, L. Davis Jr., and J. G. Melville, II, "Jupiter's Magnetic Field and Magnetosphere." (Paper presented at COSPAR Meeting, Phila., Pa., June 17, 1976a.)

21. D. E. Jones, J. G. Melville, L. Davis, Jr., and E. J. Smith, "Modeling Jupiters Magnetospheric Current Disc: Pioneers 10 and 11," EOS Trans. AGU, 57, 991 (1976). (Abstract of paper presented at Fall Meeting of the AGU, December, 1976b.)

22. E. J. Smith, L. Davis, Jr., D. E. Jones, P. J. Coleman, Jr., D. S. Colburn, and P. Dyal, "August 1972 Solar Terrestrial Events: Observations of Interplanetary Shocks at 2.2 AU," J. Geophys. Res., 82, 1077 (1977).

23. D. E. Jones and J. D. Mihalov, "Study of Static Characteristics of Jupiter's Outer Magnetosphere," EOS Trans. AGU, 58, 1218 (1977). (Abstract of paper presented at the Fall Meeting of the AGU, December 1977).

24. D E. Jones, "Magnetopause currents, multiple trapping and energetic particle flux anomalies; pioneer 10 inbound," Encyclia, 54, 106 (1977). (Abstract of paper presented at the Fall Meeting of the Utah Academy of Sciences Arts and Letters, December 1977.)

25. D. E. Jones, "Oscillations of the giant current disc surrounding Jupiter: Pioneer 10 inbound," Encyclia, 55, 164, 1978. (Abstract of paper presented at the Fall Meeting of the Utah Academy of Sciences, Arts, and Letters, November, 1978.

26. D. E. Jones, "On the phase relationship between the energetic particle flux modulation and current disc penetrations in the Jovian magnetosphere: Pioneer 10 inbound," Geophys. Res. Letters, 6, 45 (1979).

27. D. E. Jones, "Observations of Saturn's magnetic field and the magnetic interaction regions of Titan and the new satellite 1979 S-1," Encyclia, 56, 156, 1979. (Abstract of paper presented at the Fall Meeting of the Utah Academy of Sciences, Arts and Letters, November, 1979.)

28. E. J. Smith, L. Davis, Jr., D. E. Jones, P.J. Coleman, Jr., P. Dyal and C.P. Sonett, "Saturn's Magnetic Field and Magnetosphere: Pioneer 11," EOS Trans. AGU, 60, 865 (1979). (Abstract of paper presented at Fall Meeting of the AGU, December, 1979).

29. D. E. Jones, B. T. Tsurutani, E. J. Smith, R. J. Walker, and C. P. Sonett, "Observations of Titan's Magnetic Wake: Pioneer 11," EOS trans. AGU, 60, 866 (1979). (Abstract of paper presented at Fall Meeting of the AGU, December, 1979)

30. D. E. Jones, E. J. Smith, B. T. Tsurutani and L. Davis, Jr., "Magnetic Detection of the Satellite 1979 S-1 (Saturn) by Pioneer 11," EOS Trans. AGU, 60, 866 (1979). (Abstract of paper presented at the Fall Meeting of the AGU, December, 1979).

31. E. J. Smith, L. Davis Jr., D. E. Jones, P. J. Coleman, Jr., D. S. Colburn, P. Dyal, and C. P. Sonett, "Saturn's Magnetic Field and Magnetosphere," Science, <u>207</u>, 407 (1980).

32. D. E. Jones, J. G. Melville II, and M. L. Blake, "Modelling Jupiter's Current Disc: Pioneer 10 Outbound," J. Geophys. Res., <u>85</u>, 3329, (1980).

33. D. E. Jones, B. T. Tsurutani, E. J. Smith, R. J. Walker, and C. P. Sonett, "A Possible Magnetic Wake of Titan: Pioneer 11 Observations," J. Geophys. Res., <u>85</u>, 5835, (1980).

34. E. J. Smith, L. Davis, Jr., D. E. Jones, P. J. Coleman, Jr., D. J. Colburn, P. Dyal, and C. P. Sonett, "Saturn's Magnetosphere and It's Interaction with the Solar Wind," J. Geophys. Res., <u>85</u>, 5655, (1980).

35. L. Davis, Jr., E. J. Smith, D. E. Jones, P. J. Coleman, Jr., D. S. Colburn, P. Dyal, and C. P. Sonett, "Saturn's magnetic field, magnetosphere, and interaction with the solar wind," EOS Trans AGU, 61, 333, (1980). (Abstract of paper presented at Spring Meeting of the AGU, April, 1980).

36. D. E. Jones and L. G. Shirley, "Modulation of the Front Side Disc, Cross and Tail Currents in the Jovian Magnetosphere: Pioneers 10 and 11," EOS Trans AGU, <u>61</u>, 349, (1980).

37. D. E. Jones, B. T. Thomas, and J. G. Melville II, "Equatorial Disk and Dawn-Dusk Currents in the Frontside Magnetosphere of Jupiter: Pioneers 10 and 11," J. Geophys. Res., <u>86</u>, 1601, (1981).

38. D. E. Jones and B. T. Thomas, "Modeling of disc and tail currents in both the front and back regions of the magnetosphere of Jupiter: Pioneer results," EOS Trans AGU, <u>62</u>, 999, (1981). (Abstract of paper presented at Fall Meeting of the AGU, December, 1981.)

*   Copies of papers published in the Utah Academy Proceedings have been included as Appendix B

Figure Captions

Figures 1-3. Three views of the current disc required to fit the Pioneer 10 outbound data. Twisting, bending (towards parallelism with the jovigraphic equator) and a deformation in the form of a ridge having a spiralling symmetry line are required. The three views represented in the figures differ by 45° in the direction of rotation.

Figures 4-6. Three views 45° apart in the direction of rotation of the current disc required to fit the Voyager magnetic field data based upon fitting of the outbound Pioneer 10 data. An additional deformation in the form of a sprialling ridge was not needed for the Voyager data.
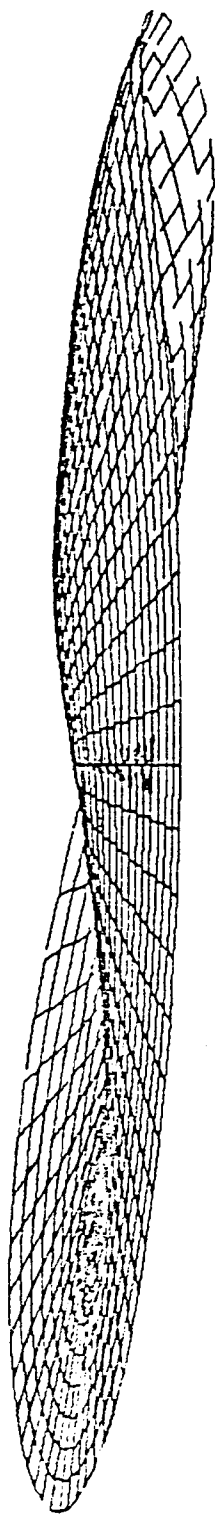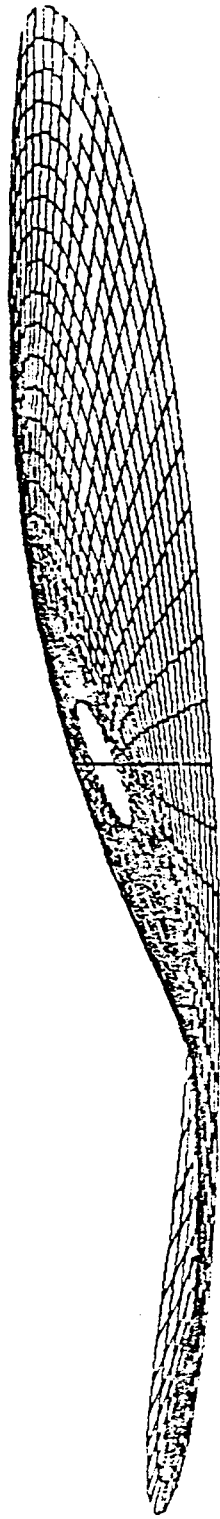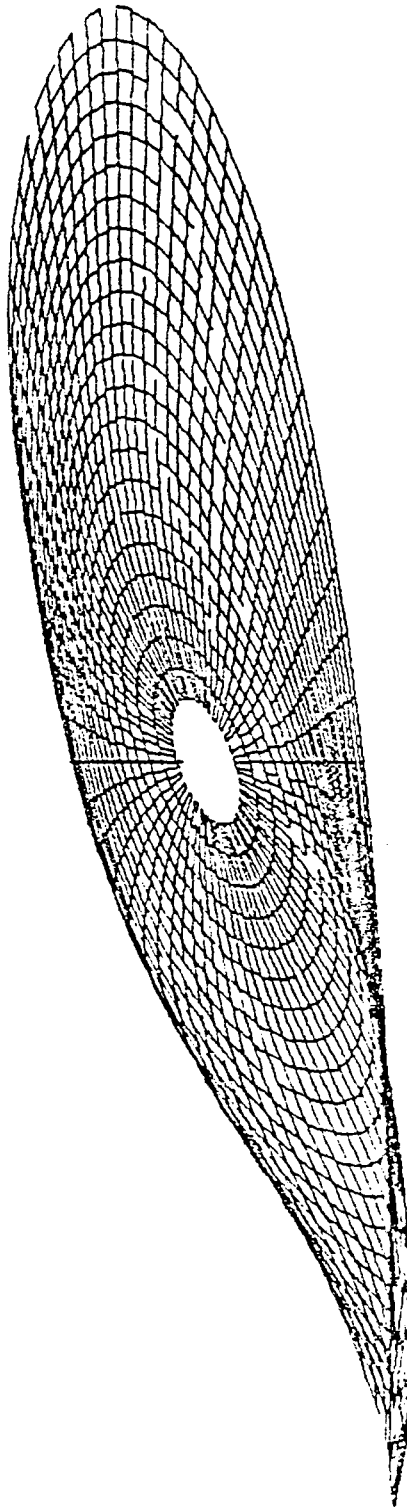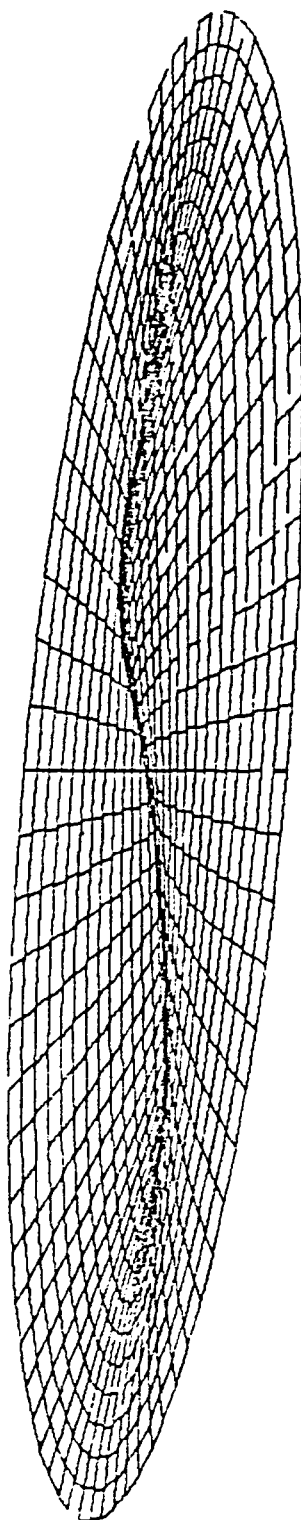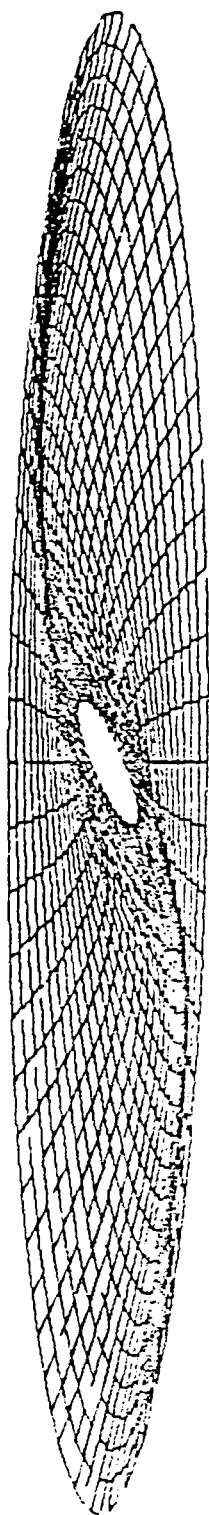
Figure 1

Figure 2

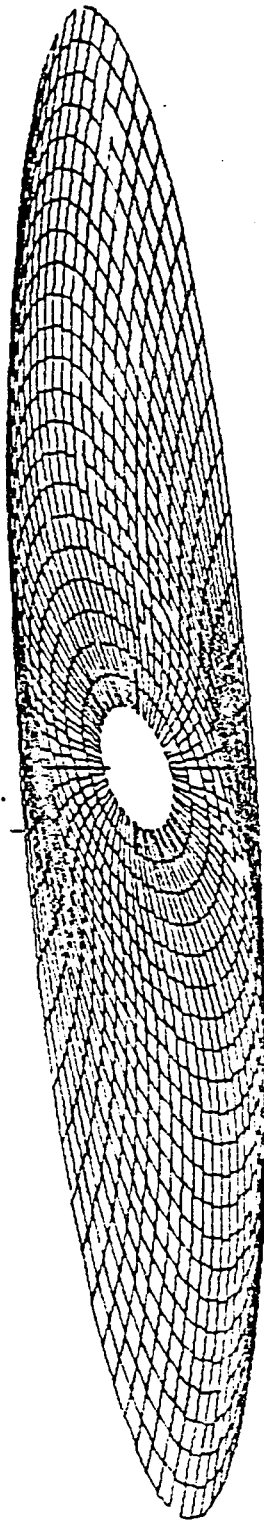Figure 3

Figure 4

Figure 5

Figure 6

Appendix A

Linear and Non-Linear Models

of Jupiter's Magnetic Field

Pioneers 10 and 11

R. Steven Turley

Brigham Young University

June 13, 1978

ABSTRACT

Two models have been used to fit Pioneer 10 and 11 magnetic field data from Jupiter. The first model consists of two offset dipoles with an exterior current ring or disc. The second model is based on a truncated spherical harmonic expansion of the magnetic scalar potential within the region of interest. Data used in the fits was obtained between 1.8 and 7.0 R_J, 32° and -50° latitude, and 0° and 360° longitude. Data for Pioneer 10 and 11 were run separately and together. In terms of an offset dipole and ring, the field is best described as a dipole with moment 4.1 Gauss-R_J^3 tilted 9.5° with respect to the spin axis and offset about .14 R_J from the planet's center. The exterior current disc has an axis roughly coinciding with that of the main dipole and an inner radius of less than 9 R_J.

We have fitted two models to Jupiter's magnetic field based on Pioneer 10 and 11 data between 1.8 and 7.0 R_J. The first model is that of two offset, tilted dipoles, with an exterior current ring. The second model is a truncated spherical harmonic expansion of the magnetic scalar potential. Data for Pioneer 10 and 11 have been fit both separately and together in the cases of both models.

The first model was chosen because of how easy it is to visualize physically. Owens Valley Radio Astronomy data (Berge and Gulkis, 1976) and measurements by others including Branson (1968), Warwick (1964) and Conway and Stannard (1972, 1976) suggest that the interior field sources are a main dipole, tilted about 10° with respect to the spin axis, and a possible anamoly at longitude 200°.

The ring current is an attempt to model the current disc which extends from about 10 to 80 R_J and its contribution to the magnetic field near the planet. It is admitedly not as good a model as, say, a current disc would be, but the contribution to the field here is so small that the ring model does a sufficiently good job.

There is justification for including all three components in the physical model. The first justification is the evidence from other sources that there are at least three contributions to the field in this region. The second justification is that there are obvious anamolies in the fit if any of these contributions are left out. Thirdly, addition of any of these three contributions to a model consisting of just the other two significantly improves the goodness of the fit.

The second model fitted to the field data is a truncated spherical harmonic expansion of the scalar potential from which the magnetic field is obtained. This model has the disadvantage of being a little harder to

visualize physically. Its advantages are that it is a more general approach, and that it is a linear formula, which makes finding a least squares fit considerably easier. The details of this approach are explained in more detail in a later section.

In the cases of both models, we were able to obtain fits to the data with from .3% to 1% deviation from the experimental fields. We found the fitted values to be quite sensitive to the segment of the trajectories used in the fit and to the weighting factors which we used. We believe the particular weighting function used for data reported in this paper to be the most reliable one. Interpretation of the differences between the various fits will be given in a later section.

MEASUREMENT UNCERTAINTY

The experimental magnetic field data was gathered by a vector helium magnetometer aboard the Pioneer 10 and 11 spacecraft. A detailed discussion of the instrument and its associated errors can be found in Smith (1975). In this section we briefly describe the experimental uncertainty in the measurements obtained and its relationship to the value of c^2 that is to be expected for each measurement range.

The magnetometer has an absolute uncertainty of less than 5% based on inflight calibration data. For the large fields measured in the experiment however, resolutions of at least $\pm 1\gamma$ were possible (.01% uncertainty). In this case the primary source of error is due to digitization. The following table was taken from information supplied by Smith (1974) and gives an indication of the variance expected in each of the magnetometer's field ranges due to quantization of the data.

Maximum Field	Digital Step Size γ/bit	c^2 (γ)
4 γ	0.015	1.88×10^{-5}
13 γ	0.052	2.25×10^{-4}
43 γ	0.167	2.32×10^{-3}
146 γ	0.569	.027
632 γ	2.46	.504
3880 γ	15.1	19.0
0.227 G	88.2	648
1.37 G	531.0	235000

c^2 is found as follows. Let ε be the digital step size and B_o be the digital value of the field, B. If B is between $B_o - \varepsilon/2$ and $B_o + \varepsilon/2$, the reported value will be B. Assume equal probability of B being anywhere in the interval. Let x be the difference between B and B_o.

$$c^2 = 1/\varepsilon \int_{-\varepsilon/2}^{\varepsilon/2} x^2 \, dx = \varepsilon^2/12$$

Note that on the average, σ is of the order of .2% of the mid-point value for each range. This should represent the lowest possible value of σ obtainable in any model fitting to the data.

This section describes the units used in the calculations and results. First the position coordinates then the magnetic field variables will be discussed.

Throughout this paper all position variables will be expressed in modified System III (epoch 1957.0) coordinates, unless noted otherwise. Spherical coordinates are expressed in terms of radius, latitude, and longitude. The radius is in meters or in R_J (Jovian Radii). Throughout this paper the value of 1 R_J = 7.08x10^7 meters has been assumed. The latitude measurements are identical to System III latitudes. The longitudes are measured from the same axis as in System III, but in a counter-clockwise direction as viewed from the North Pole rather than in a clockwise direction. The modified System III longitudes (θ') used here are related to System III longitudes (θ_{III}) by the relation

$$\theta' = 360° - \theta_{III}.$$

Dipole offsets are expressed in cartesian coordinates, using the spin axis as the z axis and the line of 0° latitude and longitude as the x axis.

The magnetic field variables are needed to express the dipole strength, the field strength, and the current in the ring of Model III. The dipole strength is expressed in Gauss-R_J^3, with R_J defined as before

$$1 \text{ Gauss-}R_J^3 = 3.55 \times 10^{23} \text{ Gauss-m}^3$$
$$= 3.55 \times 10^{19} \text{ Weber-m}$$

Magnetic field data is in γ, where $1\gamma = 10^{-5}$ Gauss. Program calculations and outputs are in Gauss (1 Gauss = 10^{-4} Weber/m^2). The currents are measured in amps.

It will be noted that our choice of a fixed planetary coordinate system differs from that of Smith (1974), in which a coordinate system fixed to the

Jupiter-Sun line for the external sources was chosen. The outer edges of the external sources is probably very strongly influenced by the solar wind. However, the dominant force shaping the near exterior field sources (which were of primary interest in this study) should be the strong planetary field. A partial justification of this assumption is in the improved fits we were able to obtain compared to those reported by Smith et al, (1976).

NON-LINEAR MODEL CALCULATIONS

In this section the formulas used to calculate the fields due to an offset dipole, a current ring, and a current disc were explained. The formula for an offset dipole is well known and hence not derived. The formula for a current loop and a current disc are derived in detail.

Dipole Field

The equation for the magnetic field due to a dipole centered at the origin is

$$\vec{B} = \mu_0/4\pi[\vec{M}/|\vec{r}|^3 - ((\vec{M}\cdot\vec{r})\vec{r})/|\vec{r}|^5]$$

where

$\mu_0 = 4\pi \times 10^{-3}$ (Gaussian units)

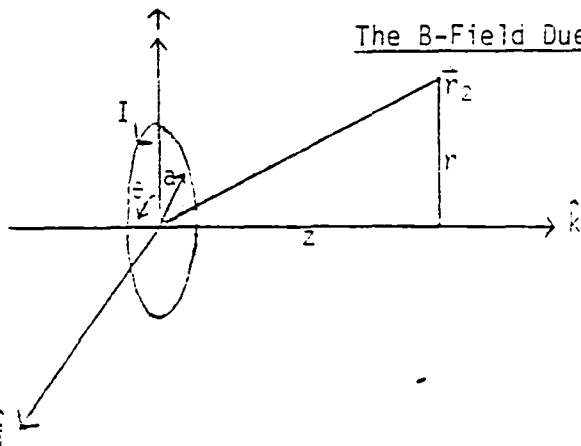$\vec{M}$ is in Gauss-R_J^3

$\vec{r}$ is in R_J

letting C be the offset of the dipole and $\overline{RC} = \vec{R} - \vec{C}$, the above equation can be expressed for an offset dipole as

$$\vec{B} = \mu_0/4\pi[\vec{M}/|\overline{RC}|^3 - ((\vec{M}\cdot\overline{RC})\overline{RC})/|\overline{RC}|^5]$$

$$B_x = \mu_0/4\pi[M_x/|\overline{RC}|^3 - ((\vec{M}\cdot\overline{RC})RC_x)/|\overline{RC}|^5]$$

$$B_y = \mu_0/4\pi[M_y/|\overline{RC}|^3 - ((\vec{M}\cdot\overline{RC})RC_y)/|\overline{RC}|^5]$$

$$B_z = \mu_0/4\pi[M_z/|\overline{RC}|^3 - ((\vec{M}\cdot\overline{RC})RC_z)/|\overline{RC}|^5]$$

The B-Field Due to a Ring Current

a = radius of loop

I is counterclockwise as viewed from the $\hat{k}$ axis.

8

It is assumed that $\bar{r}_2$ has no $\hat{j}$ component, since symmetry would seem to require that $\bar{B}$ not depend on the z coordinate of x.

The Biot-Savart Law gives $\quad \bar{B}(\bar{r}_2) = \frac{\mu_0}{4\pi} I \oint_j \frac{d\bar{\ell} \times (\bar{r}_2 - \bar{r}_1)}{|\bar{r}_2 - \bar{r}_1|^3}$.

$$\bar{r}_2 = r\hat{i} + z\hat{k} \qquad\qquad \bar{r}_1 = a\cos\phi\hat{i} + a\sin\phi\hat{j}$$

$$\bar{r}_2 - \bar{r}_1 = (r - a\cos\phi)\hat{i} - a\sin\phi\hat{j} + z\hat{k}$$

$$|\bar{r}_2 - \bar{r}_1|^3 = (r^2 - 2ar\cos\phi + a^2 + z^2)^{3/2}$$

$$= (a^2 + r^2 + z^2 - 2ar\cos\phi)^{3/2}$$

$$d\hat{\ell} = -a\sin\phi\,d\phi\hat{i} + a\cos\phi\,d\phi\hat{j}$$

$$d\bar{\ell} \times (\bar{r}_2 - \bar{r}_1) = d\phi\{a\sin^2\phi\hat{k} + z\sin\phi\hat{j} + (a\cos^2\phi - r\cos\phi)\hat{k} + z\cos\phi\hat{i}\}$$

$$= a\,d\phi\{z\cos\phi\hat{i} + z\sin\phi\hat{j} + (a - r\cos\phi)\hat{k}\}$$

$$\bar{B} = \frac{\mu_0 Ia}{4\pi} \int_0^{2\pi} \frac{z\cos\phi\hat{i} + z\sin\phi\hat{j} + (a-r\cos\phi)\hat{k}}{(a^2 + r^2 + z^2 - 2ar\cos\phi)^{3/2}}\,d\phi$$

Since the denominator is even and the dB_y is odd, but dB_x and dB_z are even, this can be written as

$$\bar{B} = \frac{\mu_0 Ia}{2\pi} \int_0^{\pi} \frac{z\cos\phi\hat{i} + (a - r\cos\phi)\hat{k}}{(a^2 + r^2 + z^2 - 2ar\cos\phi)^{3/2}}\,d\phi \qquad .$$

Let $\phi = \phi/2$.

$$\bar{B} = \frac{\mu_0 Ia}{\pi} \int_0^{\pi/2} \frac{z\cos 2\phi\hat{i} + (a-r\cos 2\phi)\hat{k}}{(a^2 + r^2 + z^2 - 2ar\cos 2\phi)^{3/2}}\,d\phi$$

$$\cos 2\phi = 1 - 2\sin^2\phi$$

$$\bar{B} = \frac{\mu_0 Ia}{\pi} \int_0^{\pi/2} \frac{(z - 2z\sin^2\phi)\hat{i} + (a - r + 2r\sin^2\phi)\hat{k}}{(a^2 + r^2 + z^2 - 2ar + 4ar\sin^2\phi)^{3/2}}\,d\phi$$

$$= G \int_0^{\pi/2} \frac{(z - 2z\sin^2\phi)\hat{i} - (a - r + 2r\sin^2\phi)\hat{k}}{(1 + \beta^2\sin^2\phi)^{3/2}}\,d\phi$$

where $\quad \beta^2 = \dfrac{4ar}{(a-r)^2 + z^2} \qquad\qquad G = \dfrac{\mu_0 Ia}{\pi[(a-r)^2 + z^2]^{3/2}}$

This involves integrals of two forms

$$A(\ell) = \int_0^{\pi/2} \frac{d\theta}{(1+\ell^2\sin^2\theta)^{3/2}} \qquad \text{and} \qquad B(\ell) = \int_0^{\pi/2} \frac{\sin^2\theta \, d\theta}{(1+\ell^2\sin^2\theta)^{3/2}} \quad .$$

$$\bar{B} = zG\left[A(\ell) - 2B(\ell)\right]\hat{i} + [G(a-r)A(\ell) + 2rGB(\ell)]\hat{k}$$

To evaluate $A(\ell)$ and $B(\ell)$ let $t=\sin\theta$ $\cos\theta = \sqrt{1-t^2}$

$$dt = \cos\theta \, d\theta \qquad d\theta = \frac{dt}{\sqrt{1-t^2}}$$

$$A(\ell) = \int_0^1 \frac{dt}{(1-t^2)^{1/2}(1+\ell^2t^2)^{3/2}} \qquad B(\ell) = \int_0^1 \frac{t^2 \, dt}{(1-t^2)^{1/2}(1+\ell^2t^2)^{3/2}}$$

$$A(\ell) = \frac{1}{\ell^3} \int_0^1 \frac{dt}{(t^2+\ell^{-2})[(t^2+\ell^{-2})(1-t^2)]^{1/2}}$$

if $a = \frac{1}{\ell}$ $b = 1$ $x = 1$ This corresponds to 17.4.51 in Abramowitz and Stegen (p. 596).

$$\sin^2\zeta = \frac{\frac{1}{\ell^2} + 1}{1(\frac{1}{\ell^2}+1)} \qquad \phi = \frac{\pi}{2} \qquad k^2 = \frac{1}{\frac{1}{\ell^2} + 1} = \frac{\ell^2}{\ell^2 + 1}$$

$$A(\ell) = \frac{1}{\ell^3} E\left[\frac{\pi}{2} \Big| \frac{\ell^2}{\ell^2+1}\right][(\frac{1}{\ell^2})(\frac{1}{\ell^2} + 1)^{1/2}] = \frac{[E(\ell^2/\ell^3+1)]}{\sqrt{\ell^2+1}}$$

$$B(\ell) = \frac{1}{\ell^3} \int_0^1 \frac{t^2 \, dt}{(t^2+\ell^{-2})[(t^2+\ell^{-2})(1-t^2)]^{1/2}} = \frac{1}{\ell^3} \int_0^1 \frac{dt}{[(t^2+\ell^{-2})(1-t^2)]^{1/2}} - \frac{A(\ell)}{\ell^2}$$

With a, b, and x as before, this also corresponds to 17.4.51 in Abramowitz and Stegen (p. 596).

$$B(\ell) = \frac{1}{\ell^3} F\left[\frac{\pi}{2} \Big| \frac{\ell^2}{\ell^2+1}\right][\frac{1}{\ell^2} + 1]^{-1/2} - \frac{A(\ell)}{\ell^2}$$

$$= \frac{1}{\ell^2\sqrt{\ell^2+1}} \left\{[K(\frac{\ell^2}{\ell^2+1})] - [E(\frac{\ell^2}{\ell^2+1})]\right\}$$

10

Where $E(\ell) = \int_0^1 (1-t^2)^{-1/2} (1-\ell t^2)^{1/2} \, dt$

is the complete elliptic integral of the second kind and

$$K(\ell) = \int_0^1 [(1-t^2)(1-\ell t^2)]^{-1/2} \, dt$$

is the complete elliptic integral of the first kind.

The Current Disc Field

The equation for the field due to a disc are found from those of the ring in a simple manner. The equation of the ring current can be written as

$$\vec{B} = I\vec{A}(r,\theta,\phi)$$

$$\text{let } dI = \frac{J_o \, dr}{r^{1.8}}$$

$$\vec{B} = J_o \int_{r_o}^{r_f} \frac{\vec{A}(r,\theta,\phi) \, dr}{r^{1.8}}$$

where r is the radius of the ring

r_o is the inner radius of the disc

r_f is the outer radius of the disc

The above integration was performed numerically, using the formula for $\vec{A}$ derived from the formula for $\vec{B}$ derived in the previous section.

SPHERICAL HARMONICS CALCULATIONS

If there are negligible currents in a region of interest, and if the electric field is slowly varying, $\nabla \times \vec{B} \sim 0$, and $\vec{B}$ can be written as the gradient of a scalar. Let U represent the magnetic scalar potential defined by $\vec{B} = -\nabla U$. Since $\nabla \cdot \vec{B} = 0$ requires that $\nabla^2 U = 0$, U must therefore satisfy Laplace's equation.

A solution to Laplace's equation in spherical polar coordinates is the familiar spherical harmonic expansion:

$$U = \sum_{\ell=1}^{\infty} \sum_{m=0}^{\ell} [r^{-\ell-1}(g_\ell^m \cos m\phi + h_\ell^m \sin m\phi) + r^\ell(\bar{g}_\ell^{-m} \cos m\phi + \bar{h}_\ell^{-m} \sin m\phi)]$$
$$P_\ell^m (\cos \theta). \tag{1}$$

Here $P_\ell^m (\cos \theta)$ are the Schmidt normalized Associated Legendre Polynomials defined by

$$P_\ell^m(x) = \left[\frac{2(\ell-m)!}{(\ell+m)!}\right]^{1/2} (1-x^2)^{m/2} \quad \frac{d^m}{dx^m} [P_\ell(x)].$$

Consider a region bounded by two concentric spheres. The contribution to the potential inside this region can be due to sources interior to the smaller sphere (interior sources), or exterior to the larger sphere (exterior sources). The coefficients $\bar{g}_e^m$ and $\bar{h}_e^m$ in the expansion of the potential due to interior sources must be zero if the potential is to be finite as r approaches infinity. Likewise, the coefficients g_e^m and h_e^m must be zero if the potential due to exterior sources is to remain finite at r=0. For this reason, g_e^m and h_e^m will be refered to as interior coefficients and $\bar{g}_e^m$ and $\bar{h}_e^m$ will be refered to as exterior coefficients. The terms with $\ell=1$ are commonly called dipole terms, those with $\ell=2$ are called quadrupole terms, and those with $\ell=3$ are refered to as octupole terms.

Spherical Harmonics

Many of the coefficients in spherical harmonic expansion can be related to parameters of our other model. In the following sections we will show how the coefficients are related to the parameters of a single offset dipole and of a current disc.

Offset Dipole

The potential due to an offset dipole of moment $\vec{m}$, at a displacement $\vec{r}$ from the dipole is: $U = \dfrac{\vec{m} \cdot \vec{r}}{4\pi r^3}$. let $\vec{M} = \dfrac{\vec{m}}{4\pi}$ ($\vec{M}$ will be in Gauss-$R_J{}^3$).
$U = \dfrac{\vec{M} \cdot \vec{r}}{r^3}$. Consider a coordinate system with an origin 0 which is different from the center of the dipole, $0'$. Let $\vec{r}_0$ be the vector from $0'$ to the point P where the potential is to be computed.
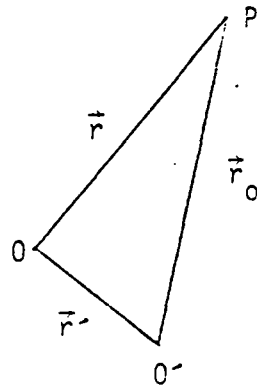
$$\vec{r}_0 = \vec{r} - \vec{r}'$$

Let
$$\vec{r}' = \eta\hat{i} + \zeta\hat{j} + \xi\hat{k}$$
$$\vec{M} = M_x\hat{i} + M_y\hat{j} + M_z\hat{k}$$
$$\vec{r} = r\sin\theta\cos\phi\,\hat{i} + r\sin\theta\sin\phi\,\hat{j} + r\cos\theta\,\hat{k}$$

Therefore,

$$U = \frac{M_x(r\sin\theta\cos\phi-\eta) + M_y(r\sin\theta\sin\phi-\zeta) + M_z(r\cos\theta-\xi)}{[(r\sin\theta\cos\phi-\eta)^2 + (r\sin\theta\sin\phi-\zeta)^2 + (r\cos\theta-\xi)^2]^{3/2}} \qquad (2)$$

13

The linear independence of the terms in the spherical harmonic expansion require that coefficients of equal powers of r in both expressions of U (Equations 1 and 2) be equal. To enable this comparison, expand the denominator of equation 2 by the binomial theorem.

After a little reduction, r_0^{-3} can be written as

$$r_0^{-3} = [r^2 + \eta^2 + \zeta^2 + \xi^2 - 2r(\xi\cos\theta + \eta\sin\theta\cos\phi + \zeta\sin\theta\sin\phi)]^{-3/2}$$

letting $\quad b = \eta^2 + \zeta^2 + \xi^2$

$$a = -2(\xi\cos\theta + \eta\sin\theta\cos\phi + \zeta\sin\theta\sin\phi)$$

$$r_0^{-3} = [r^2 + ar + b]^{-3/2} = [r^2 + c]^{-3/2} \quad \text{where } c = ar+b$$

$$[r^2 + c]^{-3/2} = \frac{1}{r^3} - \frac{3/2c}{r^5} + \frac{15/8c^2}{r^7} + \ldots$$

$$= \frac{1}{r^3} - \frac{3/2a}{r^4} + \frac{15/8a^2 - 3/2b}{r^5} + \ldots$$

Since we are only interested in dipole and quadrupole terms in the expansion, only terms up to order $1/r^4$ will be retained. Hence,

$$U = \{\frac{1}{r^3} + \frac{3}{r^4}(\xi\cos\theta + \eta\sin\theta\cos\phi + \zeta\sin\theta\sin\phi)\} \{M_x(r\sin\theta\cos\phi - \eta) +$$
$$M_y(r\sin\theta\sin\phi - \zeta) + M_z(r\cos\theta - \xi)\}$$

Equating $\frac{1}{r^2}$ terms gives

$$M_x\sin\theta\cos\phi + M_y\sin\theta\sin\phi + M_z\cos\theta = g_1^0\cos\theta + g_1^1\cos\theta\sin\theta + h_1^1\sin\theta\sin\phi$$

Therefore,

$$M_x = g_1^1$$
$$M_y = h_1^1$$
$$M_z = g_1^0$$

The terms in $\frac{1}{r}$ give

$$-M_x\eta - M_y\zeta - M_z\xi + 3(\xi\cos\theta + \eta\sin\theta\cos\phi + \zeta\sin\theta\sin\phi)(M_x\sin\theta\cos\phi + M_y\sin\theta\sin\phi + M_z\cos\theta) =$$

$$g_2^0 \left[\frac{1}{2}(3\cos^2\theta - 1)\right] + \sqrt{3}\, g_2^1 \sin\theta\cos\theta\cos\phi + \sqrt{3}\, h_2^1 \sin\theta\sin\phi\cos\theta +$$

$$\frac{\sqrt{3}}{2} g_2^2 \sin^2\theta\cos 2\phi + \frac{\sqrt{3}}{2} h_2^2 \sin^2\theta\sin 2\phi \tag{3}$$

This equality must hold for all θ and ϕ; therefore it must be valid when $\theta=0$. In this case

$$g_2^0 = -\eta M_x - \zeta M_y + 2\xi M_z$$

or, in terms of g_1^0, g_1^1, and h_1^1

$$g_2^0 = -\eta g_1^1 - \zeta h_1^1 + 2\xi g_1^0 \; .$$

The coefficients of $\sin\theta\cos\theta\cos\phi$ and of $\sin\theta\cos\theta\sin\phi$ must also be equal, if the above expression is to be valid for all θ and ϕ. This yields,

$$g_2^1 = \sqrt{3}\,\xi M_x + \sqrt{3}\eta M_z$$

or

$$g_2^1 = \sqrt{3}(\xi g_1^1 + \eta g_1^0)$$

and

$$h_2^1 = \sqrt{3}\xi M_y + \sqrt{3}\zeta M_z$$

$$= \sqrt{3}(\xi h_1^1 + \zeta g_1^0)$$

Substituting these expressions into equation (3) yields

$$\frac{\sqrt{3}}{2} g_2^2 \sin^2\theta\cos2\phi + \frac{\sqrt{3}}{2} h_2^2 \sin^2\theta\sin2\phi = -\frac{3}{2\eta} M_x\sin^2\theta - \frac{3}{2}\zeta M_y\sin^2\theta + 3M_{xy}\sin^2\theta\cos^2\phi +$$

$$3M_y\zeta\sin^2\theta\sin^2\phi + 3M_y\eta\sin^2\theta\cos\phi\sin\phi + 3M_x\zeta\sin^2\theta\cos\phi\sin\phi$$

Solving for g_2^2 and h_2^2 yields

$$g_2^2 = \sqrt{3}(\eta M_x - \zeta M_y)$$

$$h_2^2 = \sqrt{3}(\eta M_y + \zeta M_x)$$

or

$$g_2^2 = \sqrt{3}(\eta g_1^1 - \zeta h_1^1)$$

$$h_2^2 = \sqrt{3}(\eta h_1^1 + \zeta g_1^1)$$

Following the derivation by Schmidt (1934) we will find the values of $\bar{M}$ and $\bar{r}_0$ which would best represent the spherical harmonics expansion of a dipole field. Note that if the dipole were in a coordinate system with an origin at $0'$, $\xi=\eta=\zeta=0$, and all g_ℓ^m and h_ℓ^m with $\ell>1$ would be zero. To best approximate an offset dipole field, we will require that in the coordinate system centered at $0'$ $|(U_2)^2|$ be a minimum, where

$$U_2 = \sum_{m=0}^{2} (g_2^m \cos m\phi + h_2^m \sin m\phi)\ P_2^m (\cos \theta)$$

$$|(U_2)^2| = \frac{1}{5} \sum_{m=0}^{2} (g_2^m) + (h_2^m)$$

minimizing $|(U_2)^2|$ requires that $\nabla|(U_2)^2| = 0$.

In the new coordinate system

$$g_1^{0'} = g_1^0 \qquad g_1^{1'} = g_1^1 \qquad h_1^{1'} = h_1^1$$

$$g_2^{0'} = g_2^1 - (2\xi g_1^0 - \eta g_1^1 - \zeta h_1^1)$$

$$g_2^{1'} = g_2^1 - \sqrt{3}(\xi g_1^1 + \eta g_1^0)$$

$$h_2^{1'} = h_2^1 - \sqrt{3}(\xi h_1^1 + \zeta g_1^0)$$

$$g_2^{2'} = g_2^2 - \sqrt{3}(\eta g_1^1 - \zeta h_1^1)$$

$$h_2^{2'} = h_2^2 - \sqrt{3}(\eta h_1^1 + \zeta g_1^1)$$

$$5|(U_2)^2| = 5|(U_2)^2| - 2\xi(2g_1^0 g_2^0 + \sqrt{3}g_1^1 g_2^1 + \sqrt{3}h_1^1 h_2^1)$$

$$-2\eta(-g_1^1 g_2^0 + \sqrt{3}g_1^0 g_2^1 + \sqrt{3}g_1^1 g_2^2 + \sqrt{3}h_1^1 h_2^2) - 2\zeta(-h_1^1 g_2^0 + \sqrt{3}g_1^0 h_2^1 - \sqrt{3}h_1^1 g_2^2 + \sqrt{3}g_1^1 h_2^2)$$

$$+ (2\xi g_1^0 - \eta g_1^1 - \zeta h_1^1)^2 + 3[(\xi g_1^1 + \eta g_1^0)^2 + (\xi h_1^1 + \zeta g_1^0)^2 + (\eta g_1^1 - \zeta h_1^1)^2$$

$$+ (\eta h_1^1 + \zeta g_1^1)^2].$$

let $A = 2g_1^0 g_2^0 + \sqrt{3}(g_1^1 g_2^1 + h_1^1 h_2^1)$

$\quad\ B = -g_1^0 g_2^0 + \sqrt{3}(g_1^0 g_2^1 + g_1^1 g_2^2 + h_1^1 h_2^2)$

$\quad\ C = -h_1^1 g_2^0 + \sqrt{3}(g_1^0 h_2^1 - h_1^1 g_2^2 + g_1^1 h_2^2)$

16

Simplifying the above expression leads to

$$5|(U_2)^2| = 5|(U_2)^2| - 2\xi A - 2\eta B - 2\zeta C + (\xi g_1^0 + \eta g_1^1 + \zeta h_1^1)^2 + 3M^2(\xi^2+\eta^2+\zeta^2)$$

Setting the gradient of the above expression to zero requires that

$$A = 3M^2\xi + g_1^0 (\xi g_1^0 + \eta g_1^1 + \zeta h_1^1) \qquad (4)$$

$$B = 3M^2\eta + g_1^1 (\xi g_1^0 + \eta g_1^1 + \zeta h_1^1) \qquad (5)$$

$$C = 3M^1\zeta + h_1^1 (\xi g_1^0 + \eta g_1^1 + \zeta h_1^1). \qquad (6)$$

Since

$$g_1^0 A + g_1^1 B + h_1^1 C = 3M^2(\xi g_1^0 + \eta g_1^2 + \zeta h_1^1) + (g_1^{02}+g_1^{12}+h_1^{12})(\xi g_1^0 + \eta g_1^1 + \zeta h_1^1) = 4M^2(\xi g_1^0 + \eta g_1^1 + \zeta h_1^1)$$

then

$$\xi g_1^0 + \eta g_1^1 + \zeta h_1^1 = \frac{g_1^0 A + g_1^1 B + h_1^1 C}{4M^2} = D.$$

With these definitions, ξ, η, and ζ can be solved from equations (4), (5), and (6).

$$\xi = \frac{A - g_1^0 D}{3M^2} \qquad \eta = \frac{B - g_1^1 D}{3M^2} \qquad \zeta = \frac{C - h_1^1 D}{3M^2}$$

Disc

The spherical harmonic expansion of a disc can be computed from the expression for the potential on the axis of a current ring. Let z be the distance along the ring axis, and a be the radius of the ring. It is easy to show that

$$U = I/2 \left\{ 1 - \frac{z}{\sqrt{a^2+z^2}} \right\}$$

Let I have a radial dependence, $dI = \dfrac{J_0 a_0^\alpha \, da}{a^2}$

$$dU = \frac{J_0 a_0^\alpha da}{2a^2} \left\{ 1 - \frac{z}{\sqrt{a^2+z^2}} \right\}$$

The bracketed terms can be expanded to give

$$U = a_0^\alpha \int_{a_0}^{\infty} \frac{J_0}{2} \, da(a^{-\alpha} - z a^{-(1+\alpha)} + \frac{1}{2} z^2 a^{-(3+\alpha)} - \frac{3}{6} z^5 a^{-(5+\alpha)} - \ldots)$$

17

$$= \frac{a}{2} J_0 a_0 - \left(\frac{1+a}{2}\right) J_c Z + \frac{3-a}{4} Z J_c a_0^{-2}$$

If the axis of the disc is parallel to a spherical-polar axis, the spherical harmonic expansion becomes simply

$$U = \sum_{\ell=1}^{\infty} r^{\ell} A_{\ell} P_{\ell}(\cos \theta)$$

at $\theta = 0$

$$U = \sum_{\ell=1}^{\infty} Z^{\ell} A_{\ell}$$

The coefficients of Z^{ℓ} must be equal, therefore

$$A_0 = J_0 a_0$$

$$A_1 = -\left(\frac{1+a}{2}\right) J_0$$

$$A_2 = 0$$

$$A_3 = \left(\frac{3+a}{4}\right) J_0 a_0^{-2}$$

To transform the coordinates into a system not with the ring, the Addition Theorem is employed. Using Schmidt-normalized Legendre Polynomials gives the simple form

$$P_{\ell}(\cos \theta') = \sum_{m=0}^{\ell} P_{\ell}^m(\cos \theta) P_{\ell}^m \cos(\eta) \cos m (\phi-\xi)$$

where θ' is the angle made with the ring axis, and η and ξ are the angular coordinates of the ring axis in the new coordinate system. Thus

$$\sum_{\ell=1}^{\infty} \sum_{m=0}^{\ell} r^{\ell} A_{\ell} P_{\ell}^m (\cos \theta) P_{\ell}^m (\cos \eta) [\cos m\phi \cos m\xi - \sin m\phi \sin m\xi]$$

$$= \sum_{\ell=1}^{\infty} \sum_{m=0}^{\ell} r^{\ell} (\overline{g_{\ell}^m} \cos m\phi + \overline{h_{\ell}^m} \sin m\phi) P_{\ell}^m(\cos \theta)$$

16

and $A_{\ell} P_{\ell}^{m}(\cos \eta) \cos m\xi = \bar{g}_{\ell}^{m}$

$\qquad A_{\ell} P_{\ell}^{m}(\cos \eta) \sin m\xi = \bar{h}_{\ell}^{m}$

Comparing coefficients we obtain

$$g_1^0 = -\left(\frac{1+\alpha}{2}\right) J_0 \cos \eta$$

$$g_1^1 = -\left(\frac{1+\alpha}{2}\right) J_0 \sin\eta \cos\xi$$

$$h_1^1 = -\left(\frac{1+\alpha}{2}\right) J_0 \sin\eta \sin\xi$$

$$g_3^0 = \left(\frac{3+\alpha}{4}\right) J_0 a_0^{-2} \left(\frac{1}{2}(5 \cos^3\eta - 3 \cos \eta)\right)$$

Solving for J_0, a_0, η, and ξ yields

$$\xi = \tan^{-1} \frac{\bar{h}_1^1}{\bar{g}_1^1}$$

$$\eta = \tan^{-1} \left[\frac{\sqrt{\bar{h}_1^{1\,2}+\bar{g}_1^{1\,2}}}{\bar{g}_1^0} \right]$$

$$J_0 = \frac{2}{1+\alpha} \sqrt{\bar{g}_1^{0\,2}+\bar{g}_1^{1\,2}+\bar{h}_1^{1\,2}}$$

$$a_0 = \left[\left| \frac{(3+\alpha)J_0(5\cos\eta -5\cos\eta)}{8\bar{g}_3^0} \right| \right]^{1/2}$$

a_0 will be in R_J

J_0 will be in Gauss

Conclusion

In conclusion, in a current free region with stationary fields, the potential can be expressed as a linear combination of spherical harmonic functions. Using the above formulas the coefficients of these functions can be related to the model parameters of a single offset dipole and of a current disc.

DATA FITTING

Both the Non-linear and Spherical Harmonic Models were fit to the data by the means of a least squares technique. This consisted of minimizing χ^2 in both cases. Define χ^2 as

$$\chi^2 = \sum_{j=1}^{3} \sum_{i=1}^{N} \frac{(B_{ji} - \bar{B}_{ji})^2}{\sigma_i^2}$$

Where σ_i is the uncertainty in the ith set of measurements, B_{1i}, B_{2i}, B_{3i} are the respective x, y, and z components of the model B-field, and $\bar{B}_{1i}$, $\bar{B}_{2i}$, $\bar{B}_{3i}$ are the respective x, y, and z components of the experimental B-field.

The expected value of χ^2 for N data points and with n parameters in the model is 3N-n. In our analyses we accepted this value as being essentially correct, and adjusted σ_i so that a correct value of χ^2 was obtained.

Uncertainty- We assumed the variance in each measurement was equal to the sum of a known variance due to digitizing error (see Instrumentation Uncertainties) and a second source of error due to uncertainty in the spacecraft's position, instrument noise, time variations in the field, and probably other sources also. Although this second contribution to the error could not be determined experimentally, we expected it to be roughly proportional to the magnitude of $\bar{B}$ at each point. Thus

$$\sigma_i^2 = \sigma_d^2 + \alpha \, B_i^2$$

where σ_d is the standard deviation in measurements due to digitizing error. The parameter α was adjusted until an appropriate value for χ^2 was obtained.

Minimization Routines

Two different types of least-squares fitting were used in the two different models. The first method is exact, but only works if $\bar{B}$ is a linear combination of the coefficients which are being fitted. The second method is an iterative method which we used to fit the dual dipole model, where the field was not a linear combination of the parameters we were fitting.

Linear- If B_{ji} is a linear combination of the parameters to be fit, minimizing χ^2 is fairly straightforward. (See Mathews & Walker, pp. 391-2).

Let

$$B_{ji} = \sum_{m=1}^{n} C_{jim} A_m$$

where a_m are the parameters to be fit. Define a data vector, $\bar{X}$, and a measurement matrix M as follows

$$X_m = \sum_{j=1}^{3} \sum_{i=1}^{N} \frac{C_{jim}}{\sigma_i^2} B_{ji}$$

$$M_{m\ell} = M_{\ell m} = \sum_{j=1}^{3} \sum_{i=1}^{N} \frac{C_{jim} C_{ji\ell}}{\sigma_i^2}$$

The vector of the parameters, $\bar{A}$ is given by

$$\bar{A} = M^{-1} \bar{X}$$

The value σ_m^2, the variance in the $m\underline{^{th}}$ parameter is given by M_{mm}^{-1}.

Quadratic- If B_{ji} is not a linear combination of the parameters, a_m, a more sophisticated approach must be used to find the minimum of χ^2. We used a routine which provides second order convergence which was developed by Davidon (1966) and modified by Decker (1976).

Goodness of Fit- The goodness of each fit was found by computing the percent RMS (root mean square) deviation between the model and experimental fields.

RMS- In terms of χ^2, the RMS is defined as

$$RMS = \left[\frac{\chi^2}{3 \sum\limits_{i=1}^{N} \frac{1}{\sigma_i^2}} \right]^{1/2}$$

What we refer to as the % RMS deviation, δ, is defined by

$$\delta = \frac{\sum\limits_{i=1}^{3} \sum\limits_{i=1}^{N} (B_{ji} - \overline{B}_{ji})^2 / \sigma_i^2}{\sum\limits_{j=1}^{3} \sum\limits_{i=1}^{N} \overline{B}_{ji} / \sigma_i^2}$$

It should be noted in conclusion that the interpretation of least squares curve fitting needs to be done very carefully. In the cases of both our models the fits we obtained are sensitive to which data points are included in the trajectory, and which are not. In the case of Pioneer 10, for instance, the trajectory included a latitude range of only ± 13°. In the higher order spherical harmonic fits, a very good fit was possible which included a large quadrupole and octupole terms. If the resultant fit is compared to the field along the Pioneer 11 trajectory, there is a good agreement with that part of the model which is close to the Pioneer 10 trajectory, but a very poor fit in other regions.

DATA

The data used for these runs was 1-minute averages from Pioneer 10 and 11. The Pioneer 10 data was obtained between 2.8 and 6.5 R_J. It included a latitude range of $\pm$ 13° and a longitude range of 33° to 206°. The Pioneer 11 data was obtained from 1.8 R_J to 7.0 R_J, 32° to -50° latitude and 0° to 360° longitude. Unfortunately parts of both trajectories included data which appeared to have anomolies in it. Both of these anamolous segments occured during occultation by Jupiter and resulted from an uncertainty in the spacecraft orientation. Unless noted otherwise, data was fitted with this occultation data removed.

RESULTS

The following results were obtained for the non-linear model:

Model:	Pioneer 10	Pioneer 11 (R>2.8R_J)
MAIN DIPOLE		
M (Gauss $-R_J{}^3$)	$3.709 \pm .008$	$3.902 \pm .005$
Lat.	$80.71 \pm .04$	$80.79 \pm .07$
Lon.	$120.3 \pm .6$	$145.6 \pm .7$
Offset (R_J)		
C_x	$-0.105 \pm .002$	$-.114 \pm .002$
C_y	$0.009 \pm .002$	$-.004 \pm .001$
C_z	$0.095 \pm .003$	$-.018 \pm .001$
RING		
Radius (R_J)	$7.4 \pm .04$	$8.0 \pm .13$
Current ($\times 10^9$ amps)	$.021 \pm .001$	$.226 \pm .003$
Lat.	$81.0 \pm .2$	$68. \pm 1.$
Lon.	$217. \pm 3.$	$125. \pm 4.$
SECOND DIPOLE		
M (Gauss $-R_J{}^3$)	$.292 \pm .006$	$.306 \pm .006$
Lat.	$65.6 \pm .3$	$35.8 \pm .6$
Lon.	164.5 ± 2.2	$86. \pm 1.4$
Offset (R_J)		
C_x	$-.75 \pm .02$	$-.61 \pm .03$
C_y	$-.27 \pm .01$	$-.44 \pm .02$
C_z	$-.82 \pm .02$	$.29 \pm .01$
% RMS Deviation	$.449$	$.494$

For comparison, Pioneer 10 data with just one dipole and a ring, and with just one dipole are reported below.

$$x^2_{zi}$$

6.0

5.0

4.0

3.0

2.0

1.0

Pioneer 10 x^2_{zi} – Single Dipole

$$x^2_{zi} = \frac{(B_{zi} - \bar{B}_{zi})^2}{\sigma_i^2}$$

7.0   6.0   5.0   4.0   3.0   3.0   4.0   5.0   6.0   7.0
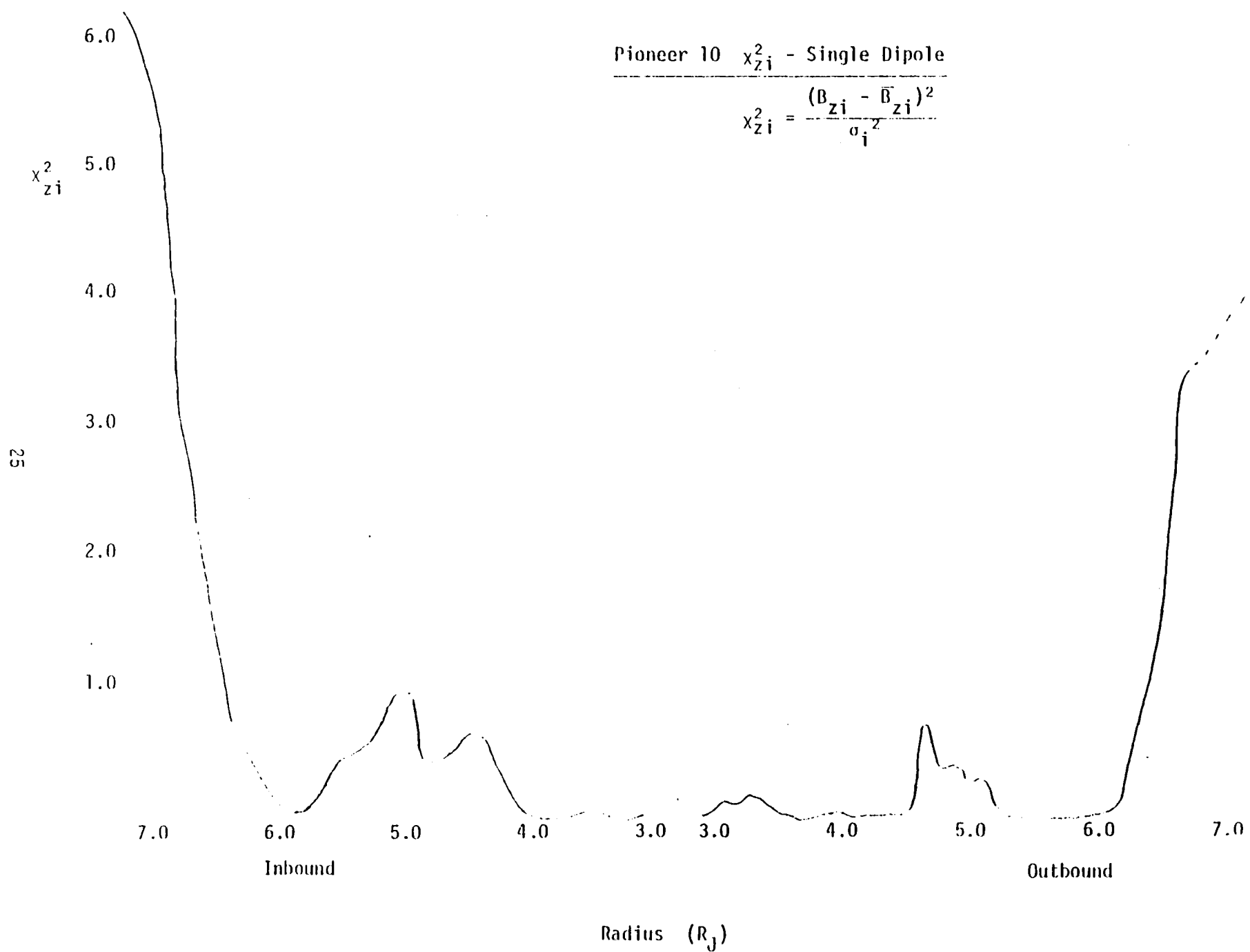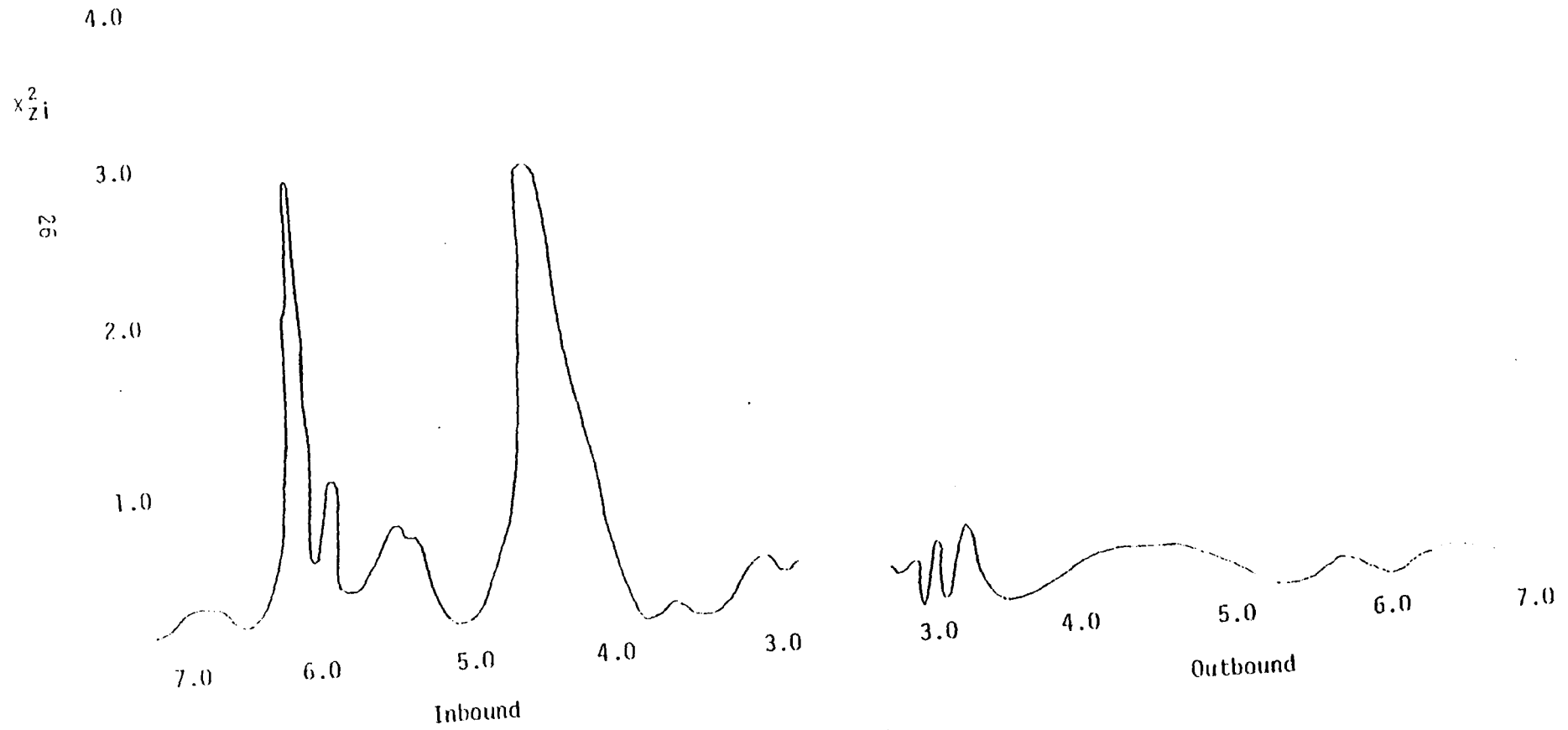
Inbound

Outbound

Radius (R_J)

Figure 1

Pioneer 10 χ^2_{zi}, Dual Dipole with Ring

$$\chi^2_{zi} = \frac{(B_{zi} - \bar{B}_{zi})^2}{\sigma_i^2}$$

Radius (R_J)

Figure 2

Pioneer 10 Fits

Dipole

$M(Gauss -R_J{}^3)$	$4.25 \pm .01$	$3.936 \pm .009$
Lat.	$79.22 \pm .04$	$79.18 = .09$
Lon.	$140.13 \pm .16$	$134.0 \pm .3$
Offset (R_J)		
C_x	$-.110 \pm .002$	$-.133 = .004$
C_y	$-.065 \pm .003$	$.006 = .003$
C_z	$.022 \pm .002$	$.031 = .004$

Ring

Radius (R_1)	$8.2 = .1$	--
Current ($\times 10^3$ amps)	$.079 = .006$	--
Lat.	$81.8 \pm .4$	--
Lon.	$172.3 = 2.$	--
% RMS Deviation	1.085	2.675

Figure 1 below shows the values of $\chi^2{}_{zi}$ as a function of the radius of Pioneer 10. The large values of χ^2 near the end points indicate a systematic deficiency due to exclusion of the ring portion of the model, since the relative effect of the ring would be largest at larger r.

Figure 2 figure shows how this effect has been eliminated in the dual dipole fit which includes the ring.

Spherical Harmonic Fit

Different numbers of interior and exterior poles were tried using the spherical harmonic approach to find the best description of the magnetic field. The results for separate runs of Pioneer 10 and 11 data are summarized in Table I.

Notice that the fits to Pioneer 10 data with more than two interior poles give values for $\bar{g}_2^m$ and $\bar{h}_2^m$ which are obviously inconsistent with the other fits as well as with the non-linear model. We believe this is due to the limited latitude range in the Pioneer 10 trajectory.

SPHERICAL HARMONICS

		Pioneer 10				Pioneer 11				Pioneer 11 R>2.8R$_J$					
Int. Poles	3	2	2	3	3	3	3	2	3	2	2	3	2	3	3
Ext. Poles	3	1	2	1	2	1	2	3	3	1	2	3	3	2	1
% RMS Dev.	.3356	.8361	.4763	.4530	.4006	.7023	.6330	.9393	.4500	.9527	.6541	.3225	.4201	.3979	.4823
G10	3.918	4.286	4.244	3.057	3.215	4.080	4.091	4.025	4.1274	4.0277	4.0283	4.0989	4.018	4.144	4.104
G11	-.9082	-.5712	-.5522	-.2511	-.2983	-.4505	-.4398	-.4887	-.4325	-.5069	-.47808	-.4252	-.4509	-.4653	-.4697
G20	.3791	.2310	.08604	.02466	-.1958	-.1059	-.1254	.06419	-.0920	.11474	.19540	-.2132	.1966	-.07854	-.04407
G21	-1.178	-.7107	-.5979	-1.942	-1.674	-.8886	-.8545	-.9848	-.726	-1.0638	-1.0519	-.8125	-1.0204	-.6932	-.8148
G22	-.2320	.2464	.3259	.6183	.6344	.3463	.3498	.4034	.3467	.3247	.41275	.3142	.5186	.3865	.3813
G30	.4996			1.681	1.193	-.3133	-.2992		-.0535			-.1730		.8089	-.6205
G31	-1.315			.5093	-.00495	-.7620	-.8303		-.71792			-1.0635		-.6116	-.5317
G32	.8220			1.884	2.011	.3540	.4105		.3853			.3735		.5581	.3998
G33	.2054			-.6966	-.5417	-.1228	-.1310		.38532			-.2172		-.03085	-.04654
H11	.4258	.5293	.5470	.5854	.5739	.6025	.5996	.4996	.5793	.61751	.59228	.5987	.5196	.5821	.6018
H21	.5173	-.5760	-.4720	2.661	2.356	-.07034	-.07621	-.04309	-.06945	-.08030	-.06207	-.0623	-.04682	-.007371	-.03650
H22	.4458	-.1406	-.08553	-.7880	-.7194	-.3534	-.3142	-.5810	-.23897	-.29898	-.29405	-.3049	-.4263	-.5073	-.4300
H31	-.9885			.06734	.3483	-.2811	-.2587		-.06567			-.2770		-.5155	-.4725
H32	1.007			2.060	1.909	-.1840	-.1870		-.11097			-.1702		-.01961	-.0807
H33	.8669			-.4213	-.4733	.2521	.3102		.29365			.0892		-.08441	+.03338
G10	65.63	-181.5	-170.2	189.0	139.9	-116.8	-122.0	-289.4	-316.9	-98.7	-107.5	-231.2	-246.0	-106	-102.9
G11	310.3	25.22	23.79	-53.59	-48.51	12.65	4.367	43.56	8.5	29.8	9.4	-3.5	-1.2	11.34	14.2
G20	-6.737		7.184		-3.821		.9166	-5.235	5.2		-4.0	4.4	-7.5	.5982	
G21	4.184		1.544		2.089		.9993	-2.615	-3.8		4.4	-.7	-.3	-1.65	
G22	.7551		1.416		-1.061		.7723	-1.742	-.7		1.6	-.9	-1.5	.294	
G30	5.467							1.904	-1.0			-.3	1.6		
G31	4.333							-.4251	-.2			-.4	-.1		
G32	-1.446							.9232	1.3			.4	.5		
G33	-.006711							-.0737	.4			.4	.2		
H11	35.08	-10.46	-1.866	-28.05	-14.28	-49.32	-39.68	39.04	-38.7	-63.2	-61.1	-47.5	15.7	-28.93	-42.28
H21	-6.730		3.899		-.5372		-.1775	-1.063	-4.9		2.4	-4.0	-.7	.4459	
H22	-6.926		.1672		.7495		-2.744	6.737	.2		-2.4	-1.0	2.0	.2114	
H31	.9774							1.205	2.9			1.4	.9		
H32	-.6201							-.2174	.2			.5	.2		
H33	.1719							-.4314	-.8			-.3	-.1		

Gauss ⎰ (G10–H33 upper block)
Y ⎰ (G10–H33 lower block)

Table I

Table II shows how the values calculated in the spherical harmonic expansions relate to the parameters in the other model.

The coefficients don't agree between the various fits in the table for a number of reasons.

1. We believe the higher order fits of Pioneer 10 data are not good because of the small latitude range in the data. The best fits of Pioneer 10 data are most likely the 2,1 and 2,2 fits.

2. Adding additional terms to a truncated series will affect the least squares fit of all of the terms in the series. We would expect the best values for g_1^0 to be in the fits using three interior coefficients.

3. There may be some secular variations in Jupiter's magnetic fields which caused a difference between the Pioneer 10 and Pioneer 11 coefficients.

For the above three reasons we decided the best description of Jupiter's average field would be provided by a fit involving three interior and three exterior poles and using combined Pioneer 10 and Pioneer 11 data. We included the exterior octupole coefficients to lend the necessary significance to the exterior dipole coefficients. Because of the axial symmetry of a disc field, we would expect the exterior quadrupole terms to be zero. Hence, it is necessary to include the octupole terms to avoid generating an asymmetry in the series by the way we've truncated it. The results of this fit are in the following table.

SPHERICAL HARMONICS

Pioneer	In/Out	Occ?	Poles int	ext	M Gauss R_J^3	Dipole Lat	Lon	CX R_J	CY R_J	CZ R_J	Rings J_0 γ	Lat	Lon
10	B	N	2	1	4.356	79.71	156.7	-.096	-.080	.028	142	81.4	157.5
10	B	N	2	2	4.314	79.6	135.3	-.084	-.068	.011	132	82.02	175.5
10	B	N	3	2	3.280	78.6	117.5	-.319	.395	.021	115	-70.1	16.4
10	B	N	3	1	3.123	78.2	113.2	-.383	.460	.067	152	-72.3	27.6
11	B	N	3	1	4.149	79.6	126.8	-.135	-.010	-.007	98	66.4	104.4
11	B	C	3	1	4.174	79.5	128.0	-.125	-.006	.001	86	66.6	108.6
11	B	C	3	2	4.210	79.8	128.6	-.109	-.000	-.004	85	73.7	111.4
11	B	N	3	2	4.158	79.7	126.3	-.129	-.011	-.010	98	71.9	96.3
11	B	N	2	3	4.085	80.1	134.4	-.152	-.005	.015	227	78.6	221.9
11	B	C	2	3	4.077	80.3	131.0	-.155	-.013	.032	189	86.3	274.2
11	B	C	2	2	4.100	79.3	128.9	-.155	-.017	.032	95	60.1	98.8
11	B	C	2	1	4.106	78.8	129.4	-.156	-.016	.022	93	54.7	115.3
11	B	N	3	3	4.190	80.1	126.7	-.109	-.012	-.006	246	82.9	102.4
10	B	N	3	3	4.044	75.6	154.9	-.134	.054	.072	246	-15.0	353.6
11	B	C	3	3	4.164	79.8	125.4	-.123	-.008	-.020	182	78.4	94.2

The computation of J_0 assumes an α of 1.6.

In/Out: B=Both I=In O=Out

Occ?: N=No Y=Yes C=Close data exluded

Table II

30

Interior Coefficients (Gauss)	Exterior Coefficients ( )
$g_1^0 = 4.099 \pm .004$	$\bar{g}_1^0 = -121 \pm 5$
$g_1^1 = -.486 \pm .003$	$\bar{g}_1^1 = 9 \pm 2$
$g_2^0 = .034 \pm .008$	$\bar{g}_2^0 = -1.1 \pm .2$
$g_2^1 = -.81 \pm .01$	$\bar{g}_2^1 = -.4 \pm .2$
$g_2^2 = .303 \pm .007$	$\bar{g}_2^2 = -.1 \pm .2$
$g_3^0 = -.04 \pm .02$	$\bar{g}_3^0 = .13 \pm .04$
$g_3^1 = -.22 \pm .03$	$\bar{g}_3^1 = -.35 \pm .04$
$g_3^2 = .41 \pm .02$	$\bar{g}_3^2 = .12 \pm .05$
$g_3^3 = -.45 \pm .02$	$\bar{g}_3^3 = -.05 \pm .03$
$h_1^1 = .526 \pm .003$	$\bar{h}_1^1 = -17 \pm 4$
$h_2^1 = -.084 \pm .007$	$\bar{h}_2^1 = 2.1 \pm .2$
$h_2^2 = -.404 \pm .006$	$\bar{h}_2^2 = .1 \pm .2$
$h_3^1 = -.04 \pm .02$	$\bar{h}_3^1 = -.30 \pm .07$
$h_3^2 = .22 \pm .02$	$\bar{h}_3^2 = .27 \pm .04$
$h_3^3 = 0.02 \pm .02$	$\bar{h}_3^3 = -.24 \pm .03$

These correspond to an offset dipole of magnitude 4.16 Gauss-R_J^3 with its axis at latitude $80.1° \pm .90$, longitude $132.7° \pm .4°$. It corresponds to a ring with $J_0 = 93\ \gamma$, with its axis at $80.7° \pm 2.3°$ latitude, $118 \pm 10°$ longitude. The percent RMS deviation was 1.1 %. With $J_0 = 93\ \gamma$, the current density would be .06 amps/meter. Assuming the ring goes from 10 R_J to 80 R_J this would mean a total current of 7×10^5 amps.

CONCLUSIONS

The two different approaches show excellent agreement in the magnitude of the total vector dipole moment. The two values obtained with the nonlinear model were 3.94 and 4.166 Gauss-R_J^3. The value obtained in the spherical harmonic approach was 4.16 Gauss-R_J^3. The dipole is tilted 9.3°, 9.2° and 9.7° from the spin axis in the three cases. The longitude of the dipole is 126.3°, 145.6°, and 132.7°. The larger difference in the longitude values is due to the high latitude of the dipole axis, as well as the lack of high latitude data on either mission, especially Pioneer 10.

The placement of the second dipole or the exact nature of the external field sources is more uncertain. The disc current tends to roughly line up with the main dipole field. The fit given by the spherical harmonic analysis agrees fairly well with the fit obtained using just a single dipole and a ring with Pioneer 10 data. This goes well with our intuitive feeling that the disc ought to line up fairly well with the main dipole field which is containing the current.

The fact that we were unable to get a consistent fit for the second dipole is probably an indication that the interior field is more complex than was assumed in our simple dual-dipole approach. Further confirmation of this is the fact that we were unable to find a good fit to the data if Pioneer 11 data with R < 2.8 R_J was included in the runs. The location of the second dipole may be further complicated by secular variations in the field sources within Jupiter. It should be noted in passing, however, that the location of the second dipole in both fits is roughly at the same longitude as the field anomolies reported by Berge and Gulkis (1976), Conway and Stannard (1972,1976) and others.

An analysis of systematic errors in the fits of the spherical harmonic and dual dipole models reveal two interesting things about the model. The first conclusion is that the current disc probably starts within 9 R_J of Jupiter. There are significant increases in the percent field deviation from the linear model between 6 and 7 R_J as would be expected in a truncated spherical harmonic expansion of the field. It would take many additional higher order terms to generate the larger increases in $\bar{B}$ one would expect near the edge of a current disc.

A second systematic anomoly in the data was noticed in both the dual dipole and spherical harmonic fits. There was a bad fit to the data at about 4.8 R_J that was particularly noticeable on both Pioneer 10 inbound and outbound. The effect was also seen, though not quite as pronounced, in the Pioneer 11 data. Such a bulge could be the result of some current flowing at about that radius since the initial assumptions in both the dual dipole and the spherical harmonic analyses are that there is no current within this region. If there is a current in this region, however, it would have to be a fairly small current compared to that in the outer ring. The current would also have to be such that the trajectory of both spacecrafts did not pass through it, since there is no evidence to support such a crossing in this region.

SUMMARY

The best average description of Jupiter's magnetic field is given by the data in Table . Physically, the field corresponds roughly to a field due to a dipole of moment M = 4.1 Gauss-RJ^3 tilted 9.5° with respect to the spin axis and at longitude 135°. The external field source is a current disc with an inner radius between 7 and 9 R_J and with an axis that roughly corresponds to the axis of the main dipole.

This type of analysis will permit better resolution of the various field sources as more field data is gathered during future Jupiter missions.

REFERENCES

Berge, G.L. and Gulkis, S. "Earth-based Radio Observations of Jupiter Millimeter to Meter Wavelengths," Jupiter, T. Gehnels, ed., University of Arizona Press, Tucson, 1976.

Branson, N.J.B.A. "High Resolution Radio Observations of the planet Jupiter," Mon. Nat. Astron. Soc., 139; 155-162, 1968.

Connely, R.G. and Stannard, D. "Non-dipole Terms in the Magnetic Fields of Jupiter and the Earth," Nature Phys. Sci., 239; 142-143, 1972.

Davidon, W.C. "Variable Metric Method for Minimization," Rep. 5590, revision 2, Argonne Nat. Lab., Lemont, Ill., 1966.

Decker, D., Brigham Young University, Personal Correspondence, 1976.

Mathews, J. and Walker, R.L. Mathematical Methods of Physics, W.A. Benjamin, Inc., Menlo Park, Cal., 1970.

Schmidt, A. "Der magnetische Mittelpunkt der Ferde und seine Bedeutung," Gerlands Beitrage Zur Geophysik, 41, 346-358, 1934.

Smith, E.J., et al. "The planetary Magnetic Field and Magnetosphere of Jupiter: Pioneer 10," J. Geophys. Res., 79; 3501-3513, 1974.

Smith, E.J., et al. "Measuring the Magnetic Fields of Jupiter and the Outer Solar System," JPL Technical Bulletin, Pasadena, Cal., 1975.

Warwick, J.W. "Radio Emission from Jupiter," An. Rev. Astron. Astrophysics, 2;1-22, 1964.

Appendix B

Papers Published in the Proceedings of the Utah Academy
of Sciences, Arts, and Letters

PIONEER 10 MEASUREMENTS OF JUPITER'S MAGNETIC FIELD

D. E. Jones,[1] E. J. Smith,[2] L. Davis, Jr.,[3]
D. S. Colburn,[4] P. J. Coleman, Jr.,[5]
P. Dyal,[4] and C. P. Sonnett[6]

After a flight of 642 days, Pioneer 10 passed the planet Jupiter at a distance of 2.84 Jupiter radii (RJ) at 0233 U.T. (Local Jupiter) on December 4, 1973. During the period November 30 through December 12 a vector helium magnetometer obtained measurements of the Jovian magnetic field. The purpose of this paper is to provide the preliminary results of these measurements.

Pioneer 10 approached Jupiter at about 6.5° south planetocentric latitude (November 30) at a Sun-Jupiter-Pioneer angle of 35°. A single bow shock crossing was observed inbound at 108 RJ (Figure 1). The magnetic

PIONEER 10 ENCOUNTER
JOVIAN FIELD MAGNITUDE
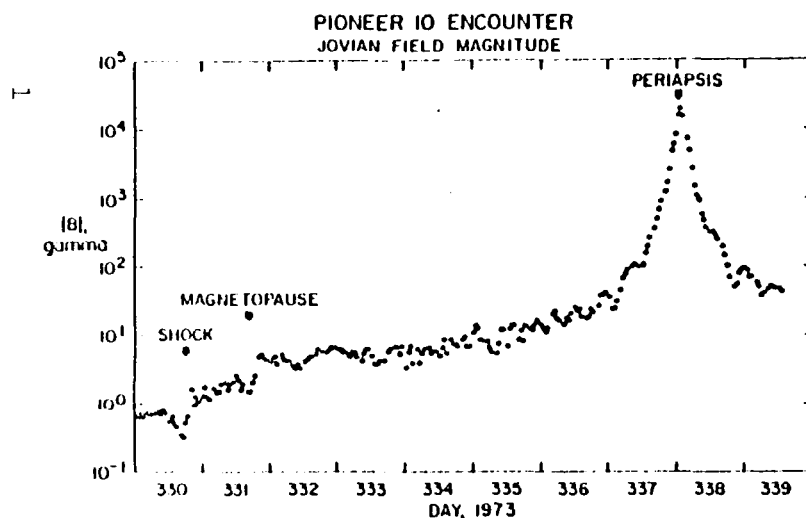
Figure 1. Five-minute averages of the field magnitude through periapsis.

1. Brigham Young University, Provo, UT
2. Jet Propulsion Laboratory, Pasadena, CA
3. California Institute of Technology, Pasadena, CA
4. Ames Research Center, Moffett Field, CA
5. University of California, Los Angeles, CA
6. University of Arizona, Tucson, AZ

field jumped from 0.5 to 1.5γ (10^{-5} gauss), and the magnetosheath fields behind the shock varied irregularly in magnitude and direction. Waves were observed in the field propagating upstream prior to the crossing of the shock. The interplanetary field direction outside the shock was such that energetic particles could propagate upstream to the spacecraft as observed by the radiation detectors.

The magnetopause was observed at 96 RJ, which was earlier than expected based upon a simple scaling of the corresponding Earth geometry (see Figure 2). This implies either a standoff distance that is relatively small as compared to Earth or else an outward motion of the magnetosphere. At the magnetopause the field jumped abruptly to 5γ. The corresponding magnetic energy density just inside the magnetosphere (10^{-10} ergs/cm^3) would appear to be insufficient to withstand the pressure of a nominal shocked solar wind (estimated to be 5×10^{-10} ergs/cm^3), or else the plasma density was much less than the nominal value of 0.2 cm^{-3}. If the solar wind density was nominal, then this implies that the principal magnetosphere pressure was due to a $\beta \simeq 4$ plasma inside the magnetosphere. A lower solar wind density implies an outward motion of the magnetosphere.

The field inside the magnetosphere exhibited a persistent southward component. Hence, the field lines were probably closed and the orientation of the dipole source at the planet was roughly parallel to Jupiter's spin axis, as inferred from radio astronomy measurements. The field magnitude remained near 5γ from 90 RJ to about 50 RJ, but was very irregular, with frequent dips to 1γ or below occurring.

The field in the outer magnetosphere was strongly distended such that its direction was elongated parallel to the equator. There was no well-defined orientation of the field into magnetic meridian planes. Referring the field vector to a Solar-Jupiter (SJ) coordinate system ($\hat{X} = \hat{S}$, $\hat{S}$ from Jupiter towards the sun; $\hat{Y}$ = normalized $\hat{J} \times \hat{S}$, $\hat{J}$ parallel to the spin axis of Jupiter; and $\hat{Z}$ completes the right-handed system) it was noted that much of the time the X and Y components were of opposite polarity, suggesting a spiraling of the meridional planes of B due to plasma effects causing the fields in the outer magnetosphere to lag behind those closer to the rapidly rotating planet. There was a frequent interchange of polarities, and occasionally there were periods when they were the same polarity. The X component was usually negative and the Y component usually positive. Hence, the spacecraft was probably below the symmetry plane most of the time. The occasional coupled X and Y polarity reversals suggest that at times the symmetry plane passed underneath the spacecraft. These results and the abnormally thin inbound magnetosheath are consistent with the existence of a relatively flat, "disclike" outer magneto-
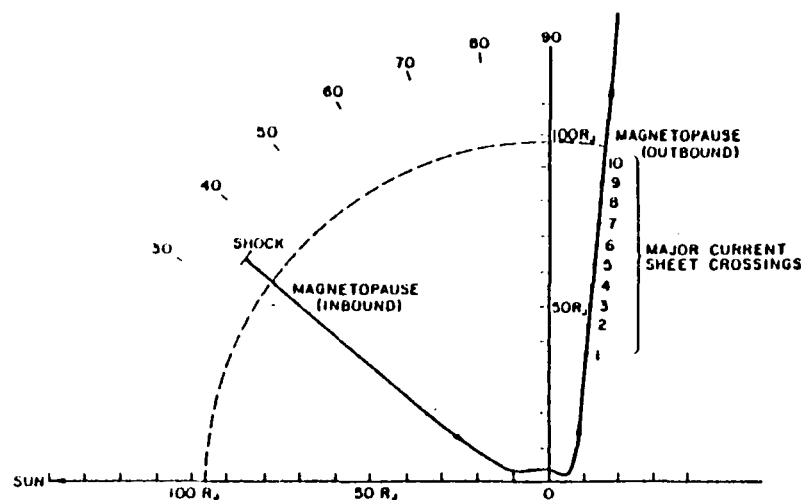
Figure 2: Trajectory plot of the Sun-Jupiter-Pioneer angle showing bow shock and magnetopause crossings. Also shown are the relative positions of the current sheet crossings.

sphere. Such a disclike field requires the presence of a current sheet roughly in the symmetry plane, and it is tempting to infer that the occasional dips in the field magnitude to $\leq 1\gamma$ may have resulted from the up and down movement of this sheet current past Pioneer 10, perhaps in response to changes in the solar wind, etc.

The field strength began to rise monotonically at about 25 RJ, and periodic variations in field direction having a 10-hour period were noted, indicating entry into the inner magnetosphere. Shortly thereafter, periodic effects in field magnitude became discernible, which appeared to correlate well with the changing magnetic latitude of Pioneer based upon the nominal radio astronomy values for the longitude and inclination of the north magnetic pole. The maximum field strength measured was 0.18 gauss, corresponding to a magnetic moment of about 4 gauss-RJ³.

The passage outbound through the magnetosphere was at a Sun-Jupiter-Pioneer angle of ≈ 100° at 0530 hours local time (Figure 2). The field was much more regular than during the inbound portion, with clear evidence of 10-hour periodicities out to 90 RJ. As the radial distance increased towards 90 RJ, the field again became strongly extended-- principally in a radial direction, so that it tended to lie parallel to the equatorial plane. The field lay nearly in the local meridian plane in the inner magnetosphere, but a systematic deviation of tens of degrees
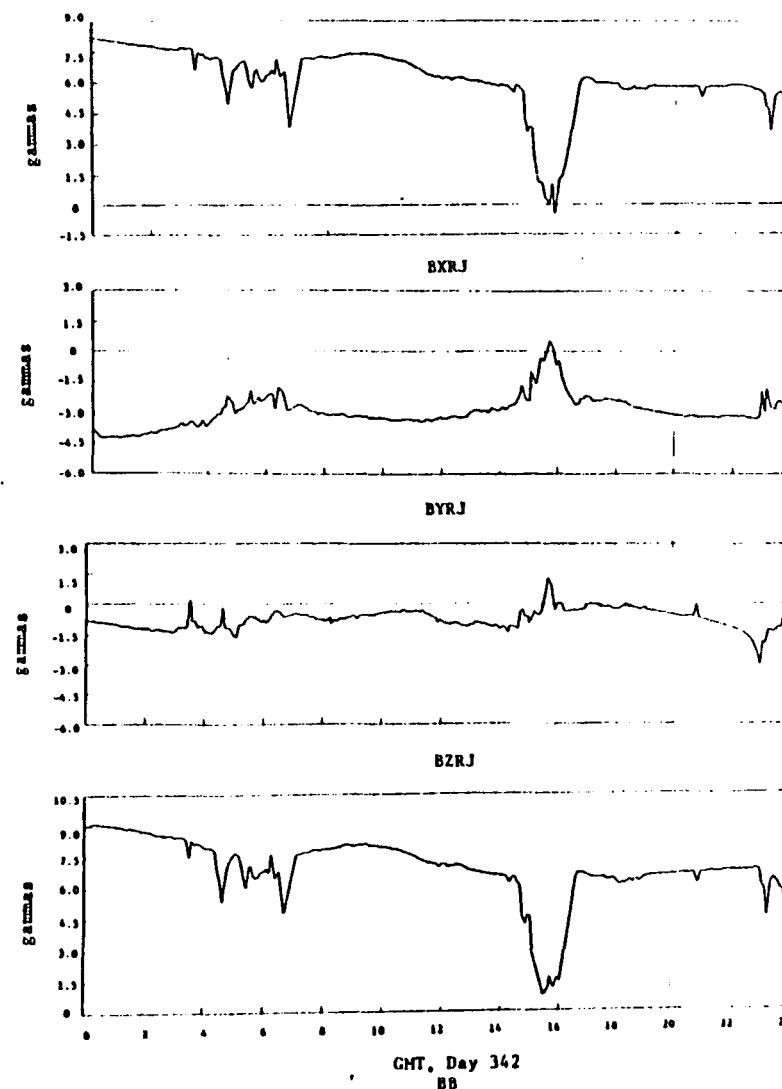

Figure 3: A portion of the magnetic field data of day 342. The observed changes in magnitude and direction are consistent with the passage of the spacecraft into a current sheet.
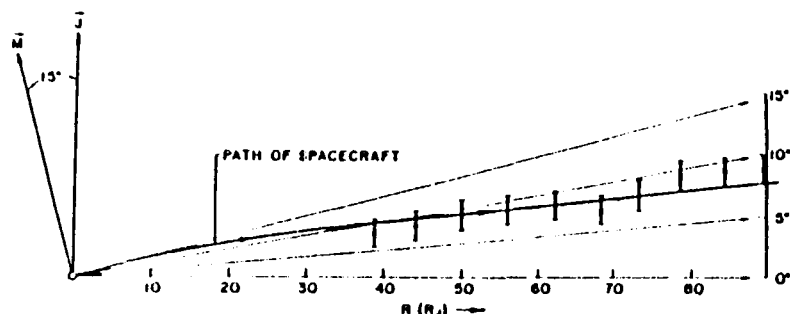
Figure 4: Planetocentric R-Latitude plot of the estimated position and extent of each current sheet crossing.

developed towards the antisolar direction, again consistent with the apparent spiralling of the field seen inbound.

Dips in the field strength with occasional partial reversals in the field components occurred at 10-hour intervals similar to the one displayed in Figure 3 (see also Figure 2). The planetocentric (rotating) coordinate position of the estimated centroids and latitudinal and longitudinal extents of these dips are displayed in Figures 4 and 5. Figure 6 shows an idealized representation of the current sheet required to explain the field dips and reversals observed during the outbound passage. Pioneer crossed the magnetopause on the outbound pass at 98 RJ, a location consistent with a cylindrically symmetric, disclike shape for the magnetosphere near the equatorial region (Figure 2).

Observations of Jupiter's magnetic field in the radial range 2.84 to 6.0 RJ were used to obtain a best least squares fit planetary dipole. During this portion of the trajectory, the standard planetocentric (JG) latitude (LATJG) and longitude (LONJG) varied from -13° to +13° and 179° CW to -46° (or 181° to 314° in System III) respectively. The corresponding dipole is characterized as follows:

Moment

M = 3.867 Gauss RJ³

MLATJG = 78.69°

MLONJG = 135.18°
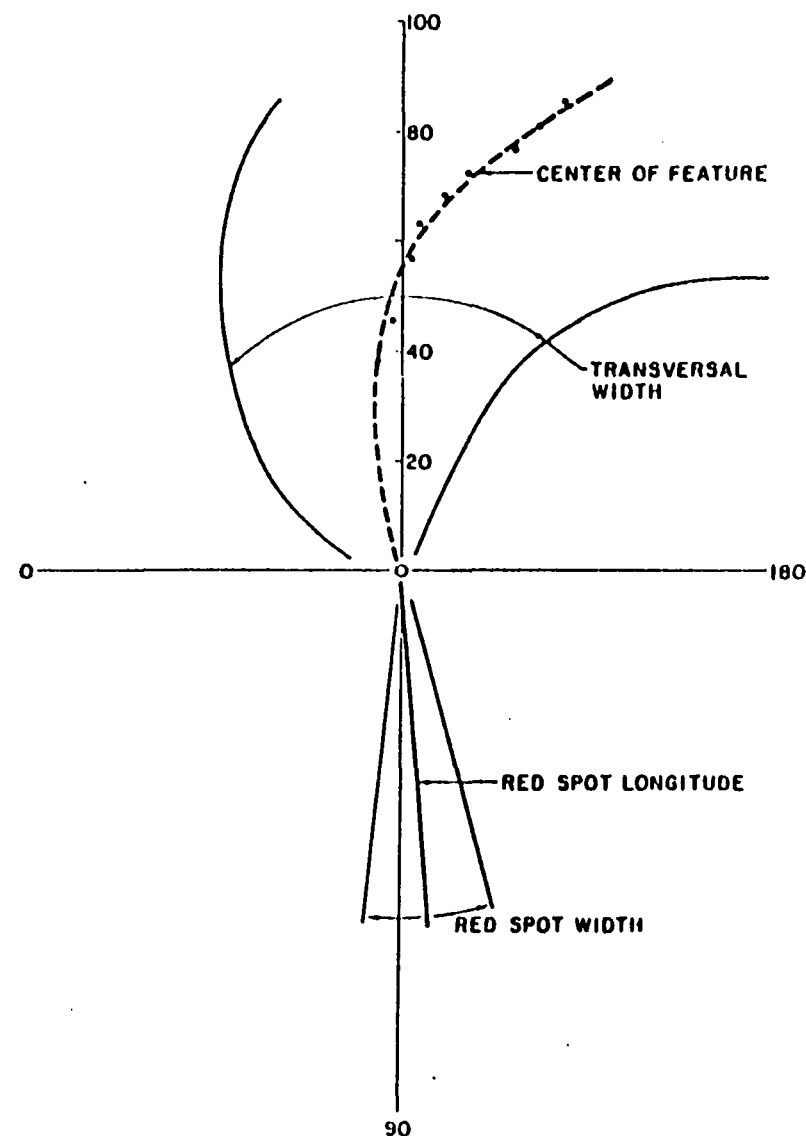
= 224.42° System III

Figure 5: Planetocentric R-Longitude plot of the estimated centroid position of each current sheet crossing and the estimated average variation of the longitudinal extent of the traversal into the sheet.
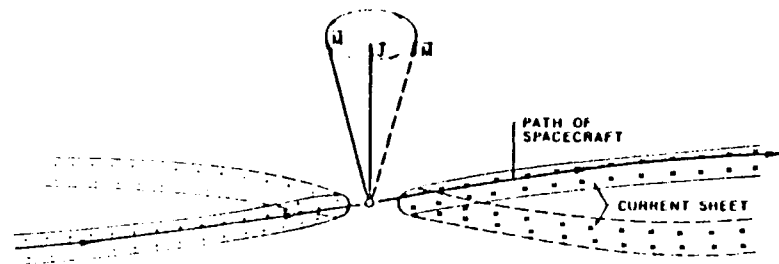
Figure 6: An idealized symmetric current sheet model inferred from the observed outbound field data.

Offset

$$CX = -.145 \text{ RJ}$$
$$CY = +.030 \text{ RJ}$$
$$CZ = +.070 \text{ RJ}$$

$$VARMXYZ = 1.08 \times 10^{-2} \text{ Gauss}^2$$
$$VARBXYZ = 4.63 \times 10^{-6} \text{ Gauss}^2$$

where $VARMXYZ$ is the rms of the component variances of M, etc. (Note that these values differ slightly from those reported earlier by Smith, et al., 1974)

In the range from 2.84 to 6.0 RJ, the off-center, tilted dipole derived above and by Smith, et al. (1974), fits the Pioneer 10 magnetometer data observed over this range to within about 3.5% of the field. The maximum surface field predicted by this model is nearly 12 Gauss, which is consistent with the maximum field strength required by the observed decametric radiation.

Acknowledgments

We express our gratitude to A. M. A. Frandsen, B. T. Tsurutani, J. Mannan, F. Barker, B. V. Connor, G. T. Foster and J. Van Amersfoort of JPL, for their dedication and support in preparation for, and during, encounter. We are also grateful to J. G. Melville and the BYU IBM 7030 operation's personnel for their outstanding support during some of the computational phases of this work related to the dipole moment of Jupiter.

References

Smith, E. J., L. Davis, Jr., D. E. Jones, D. S. Colburn, P. J. Coleman, Jr., P. Dyal, and C. P. Sonett. *Science 183*, 305 (1974).

A STUDY OF SINGLE AND DUAL DIPOLE MAGNETIC FIELD MODELS FOR JUPITER: PIONEER 10

Douglas E. Jones and John G. Melville

Brigham Young University

The results of a nearly real time analysis of the magnetic field data from Pioneer 10 have been reported previously (Smith, et al., 1974). The purpose of this note is to report an analysis of the near-Jupiter data covering roughly the same range of trajectory parameters but using as much of the data in this interval as possible. In addition to recomputing a best 3-parameter fit (minimum variance of M), we also computed best 6-parameter and 12-parameter fits (minimum variance of B) to the data. In the 12-parameter, or dual, dipole model, we have followed a suggestion by Conway and Stannard (1972) which they proposed to explain an anomaly seen in the radio astronomy linear polarization data at approximately System III longitude 220°. The second dipole is postulated to lie near the surface of the planet.

The two basic techniques used to obtain the best model parameters are related to the well-known equation for the magnetic field of an offset dipole,

$$B = -\frac{m}{(RC)^3} + 3\frac{m \cdot RC}{(RC)^5} RC \qquad (1)$$

where $RC = R - C$

  R = position vector of Pioneer relative to a planet fixed (rotating) coordinate system

  C = offset of dipole

This can be written in matrix form as

$$(B) = (A)(M) \qquad (2)$$

or, alternatively

$$(M) = (A)^{-1}(B) \qquad (3)$$

where

$$(A)^{-1} = \frac{3}{2(RC)^2}\begin{bmatrix}(RCX)^2 - 2/3(RC)^2 & (RCX)(RCY) & (RCX)(RCZ) \\ (RCX)(RCY) & (RCY)^2 - 2/3(RC)^2 & (RCY)(RCZ) \\ (RCX)(RCZ) & (RCY)(RCZ) & (RCZ)^2 - 2/3(RC)^2\end{bmatrix} \quad (4)$$

In the M method, the dipole offset C is varied (i.e., 3 parameters) until the rms M variance is minimized using equation (3) above. The B method requires that both M and C be varied (i.e., 6 parameters) until the rms B variance is minimized using equation (2). If the measured field is due to a simple offset dipole, the two methods should give nearly the same "best fit" dipole. However, if the disagreement is outside of the expected experimental error, then the source cannot be a simple dipole and the 6-parameter model should be the best. The rms B variance for each model can be used as a quantitative means of determining the best model.

In computing the variances, we first transformed the measured B from a Pioneer Inertial system (PI) into a planet fixed rotating coordinate system (JG). Interpolation of the trajectory data accurate to at least four decimal places was used to obtain the values of R corresponding to the midtime of each data sample. The observations of Jupiter's magnetic field over the approximate radial range 2.84 to 6.0 Jovian radii (RJ), the System III latitude range -13° to +13°, and longitude range 181° to 314° were used in the present analysis as before.

Using the M method, the single offset dipole that gives the best least squares 3-parameter fit to the Pioneer 10 magnetometer data used has the following parameters:

$$M = 3.867 \text{ Gauss RJ}^3$$
$$MLATJG = 78.69°$$
$$MLONJG = 135.18°$$
$$CX = -.145 \text{ RJ}$$
$$CY = +.030 \text{ RJ}$$
$$CZ = +.070 \text{ RJ}$$
$$\text{rms var } M = 1.08 \times 10^{-2}$$
$$\text{rms var } B = 4.63 \times 10^{-6}$$

The major difference between this dipole and that reported earlier (Smith, et. al., 1974) results from the use of ten-minute averages which have been corrected for an error in the roll attitude of the spacecraft and for an electronic phase lag occurring in the magnetometer.

The variable metric minimization program developed by Davidon (1966) was used in the model studies based upon the rms variance of B

(i.e., the 6- and 12-parameter models). The best least squares fit single offset dipole model obtained using this method has the parameters:

$$M = 4.07 \text{ Gauss } RJ^3$$
$$MLATJG = 78.61°$$
$$MLONJG = 139.8°$$
$$CX = -.125 \text{ RJ}$$
$$CY = -.038 \text{ RJ}$$
$$CZ = + .051 \text{ RJ}$$
$$\text{rms var } B = 1.05 \times 10^{-6}$$

Following the suggestion by Conway and Stannard (1972), we have increased the degree of complexity of the models by allowing for a second dipole. The dual dipole model that fits the data best has the parameters:

First Dipole

$$M = 4.022 \text{ Gauss } RJ^3$$
$$MLATJG = 80.08°$$
$$MLONJG = 133.60°$$
$$CX = -.200 \text{ RJ}$$
$$CY = -.03386 \text{ RJ}$$
$$CZ = + .06812 \text{ RJ}$$

Second Dipole

$$M = .0655 \text{ Gauss } RJ^3$$
$$MLATJG = 12.53°$$
$$MLONJG = 141.5°$$
$$CX = -.8221 \text{ RJ}$$
$$CY = + .4609 \text{ RJ}$$
$$CZ = -.1184 \text{ RJ}$$
$$\text{rms var } B = 7.97 \times 10^{-7}$$

One notes that the second dipole is at about .95 RJ, and the offset in the equatorial plane is at about System III longitude 209.3°.

Both of the B models fit the data significantly better than does the first or M model. However, the model which gives the best fit is clearly the one which includes a second dipole. One notes that the tilts of all of the models agree reasonably well with values derived from observations of the variation in radio intensity (Berge 1973) and from observations of Jupiter's decimetric radiation (Roberts and Komesaroff 1965). The dual dipole model also appears to be consistent with an interpretation of the polarization anomaly suggested by Conway and Stannard (1972). This

model also has a System III longitude for the main dipole which is most consistent with predictions based upon the radio measurements (Berge 1973), although there is still an apparent discrepancy of about 3°, or 1.3%.

It is difficult to justify the presence of a dipole source so near the surface of the planet. Other more complicated, but physically more reasonable, field configurations for the anomaly are possible, but most are far more difficult to work with in studies of this kind. If subsequent observations by Pioneer 11 confirm the existence of an interior field source near the surface of the planet, considerable information regarding the dynamo origin of planetary fields in general, and the structure of the interior of Jupiter in particular, will be obtained from these data.

Acknowledgments

References

Berge, G. E. "The Position and Stokes Parameters of the Integrated 21 cm Radio Emission of Jupiter and their Variation with Epoch and Central Meridian Longitude." Preprint No. 17 of the Owens Valley Radio Observatory, 1973.

Conway, R. G., and D. Stannard. *Nature Phys. Sci.* 239, 142 (1972).

Davidon, W. C. "Variable Metric Method for Minimization." Report No. 5990 (rev. 2), Argonne National Laboratories, 1966.

Roberts, J. A., and M. M. Komesaroff. *Icarus* 4, 127 (1965).

Smith, E. J., L. Davis, Jr., D. E. Jones, D. S. Colburn, P. J. Coleman, Jr., P. Dyal, and C. P. Sonett, *Science* 183, 305 (1974).

PRELIMINARY MODEL STUDIES OF THE MAGNETOSPHERE OF JUPITER: PIONEER 10

Douglas E. Jones and John G. Melville
Brigham Young University

Introduction

The Pioneer 10 spacecraft passed within 2.84 Jovian radii (R_j) of the planet Jupiter on December 4, 1973. Extensive observations of the Jovian magnetic field and its interaction with the solar wind plasma were made while the spacecraft was within about 100 R_j of the planet. The magnetosphere was found to be severely stretched because of the presence of an intense current sheet, which was particularly evident during the outbound passage of Pioneer 10 near the dawn terminator (Smith, et al., 1974). Plots of the angle between the orientation of the outbound field and the radius vector from the planet to the spacecraft showed a strong tendency for the field to become radial at large distances from the planet (see Figure 8, Smith, et al., 1974). A similar trend has also been seen in both the inbound and outbound Pioneer 11 data (Smith, et al., 1975; Jones, et al., 1975). We report here some preliminary work on a mathematical model of the magnetosphere of Jupiter which is based upon the Pioneer 10 outbound data. A preliminary model study related to the outbound Pioneer 10 data has also been reported by Goertz, et al., (1974). However, we have noted some fundamental conceptual errors in their study, and it is also the purpose of this paper to report a correction of this earlier analysis. We will also discuss some of the implications of the radial field configuration inferred from the Pioneer 10 and 11 data.

The Method

Since it is always true that

$$\nabla \cdot \vec{B} = 0,$$

one can represent $\vec{B}$ by an expression of the form

$$\vec{B} = \nabla f \times \nabla g,$$

where f and g are scalar functions of the coordinates that are sometimes referred to as Euler potentials (Euler, 1769; Truesdell, 1954; Stern, 1966). The utility of this manner of representing $\vec{B}$ lies in the fact that since $\vec{B}$ is tangent to the intersection of the surfaces $f =$ constant and

$g =$ constant, this affords a direct method of evaluating the shape of the lines of force. For example, for a dipole in spherical coordinates we have

$$f_D = \frac{M \sin^2 \theta}{\rho},$$

where $\rho = R/R_j$, and

$$g = \phi.$$

(In cylindrical coordinates, ρ will represent the dimensionless component of $\vec{R}$ that is perpendicular to the axis of the dipole.) The f function can be easily manipulated into the well-known constant L representation of a dipole field line, namely

$$\rho = L \sin^2 \theta.$$

Although the law of superposition holds for magnetic fields, this is not generally true for the functions f and g, i.e.,

$$\nabla F \times \nabla G = \nabla \left(\sum_i f_i \right) \times \nabla \left(\sum_i g_i \right) \neq \sum_i (\nabla f_i \times \nabla g_i).$$

Alternatively, one notes that

$$\nabla f \times \nabla g = \nabla \times (f \nabla g),$$

so that the vector potential $\vec{A}$ is related to the f and g functions through

$$\vec{A} = f \nabla g.$$

For axi-symmetric fields, f is independent of ϕ and $g = \phi$. The vector potential in spherical coordinates is then

$$\vec{A}_{sphr.} = \frac{f(\rho, \theta)}{\rho \sin \theta} \hat{\phi}.$$

and in cylindrical coordinates,

$$\vec{A}_{cyl.} = \frac{f(\rho, z)}{\rho} \hat{\phi}.$$

For axi-symmetric fields, or f functions sharing the same g function, one writes

$$\vec{A} = \sum_i f_i \nabla g.$$

or, alternatively,

$$\vec{B} = \nabla \times \left(\sum_i f_i \nabla g \right) = \nabla \left(\sum_i f_i \right) \times \nabla g.$$

We write with B_D being the dipole field,

$$\vec{B} = \vec{B}_D + \vec{B}_1 + \vec{B}_2,$$

or

$$\vec{B} = \nabla(f_D + f_1) \times \nabla g_1 + \nabla f_2 \times \nabla g_2,$$

so that the perturbation field $\vec{B}_p$ is given by

$$\vec{B}_p = \vec{B} - \vec{B}_D$$
$$= \vec{B}_1 + \vec{B}_2$$
$$= \nabla f_1 \times \nabla g_1 + \nabla f_2 \times \nabla g_2.$$

B_1 represents the axi-symmetric portion of the perturbation field and B_2 the component contributing to the spiraling.

Spherical Polar Coordinate Model

In spherical coordinates we have

$$\vec{B}_1 = \frac{1}{\rho^2 \sin\theta}\frac{\partial f_1}{\partial\theta}\hat{r} - \frac{1}{\rho\sin\theta}\frac{\partial f_1}{\partial\rho}\hat{\theta}$$

$$\vec{B}_2 = -\frac{k}{\rho\sin\theta}\frac{\partial f_2}{\partial\theta}\hat{\phi}.$$

Since there is clearly spiraling of the field (Smith, et al., 1974), we have written

$$g_p = g_1 + g_2$$
$$= \phi + k\rho,$$

where $k\rho$ represents the spiraling. Because B_1 and B_D share the same g function, and therefore superposition holds for the respective f functions, we will concentrate on these components of the field only. The function $F = f_1 + f_D$ will then represent meridional plane projections of the measured field.

In deriving an f_1 function, we start with a component of the perturbation field whose functional form may be easily deduced from the data. Since the radial component of the field decreased and at times reversed, which is consistent with passage into a thin current sheet (Smith, et al., 1974), a functional form for b_ρ that is consistent with these factors (see also Bird, 1975) is

$$b_\rho = \frac{A}{\rho^a}\tanh\frac{\cos\theta}{\cos\theta_0}$$

$$= \frac{1}{\rho^2\sin\theta}\frac{\partial f_1}{\partial\theta}.$$

Then

$$f_1 = -\frac{A\cos\theta_0}{\rho^a\,2}\left[\log\cosh\frac{\cos\theta}{\cos\theta_0} + C(\rho)\right]$$

and

$$b_\theta = -\frac{1}{\rho\sin\theta}\frac{\partial f_1}{\partial\rho}$$

$$= \frac{(a-2)A\cos\theta_0}{\rho^a\sin\theta}\left[\log\cosh\frac{\cos\theta}{\cos\theta_0} + C(\rho)\right]$$

$$- \frac{A\cos\theta_0}{\rho^{a-1}\sin\theta}\frac{\partial C(\rho)}{\partial\rho}.$$

At $\theta = \pi/2$,

$$b_\theta = \frac{(a-2)A\cos\theta_0}{\rho^a}C(\rho) - \frac{A\cos\theta_0}{\rho^{a-1}}\frac{\partial C}{\partial\rho}.$$

For

$$C(\rho) = \frac{C}{\rho^b}$$

we have

$$b_\theta = \frac{AC\cos\theta_0}{\rho^{a+b}}(a - 2 + b).$$

The f function corresponding to the axi-symmetric portion of the perturbation field is then given by

$$f_1 = -\frac{A\cos\theta_0}{\rho^a\,2}\left[\log\cosh\frac{\cos\theta}{\cos\theta_0} + \frac{C}{\rho^b}\right].$$

From the Pioneer 10 outbound data we find that the constants for f_1 are approximately

$$a = 1.70,$$
$$b = 1.10,$$
$$A = 7700.$$

$$C = 770,$$

$$\cos \theta_0 = 0.025.$$

Although fitting the Pioneer 10 outbound data quite well, this F function exhibited rather anomalous behavior at high latitudes. Since the expression for b_μ can include additional functions of θ which are small near $\theta = \pi/2$ (i.e., functions of $\cos \theta$), one could write

$$b_\mu = \frac{A}{\rho^a} \tanh \frac{\cos \theta}{\cos \theta_0} + \cos \theta \, h(\rho, \theta).$$

Following this lead, alternate functions can be derived. One of several which fit the data reasonably well is

$$f_1 = - \frac{A \cos \theta_0}{\rho^{a-2}} \left[\log \cosh \frac{\cos \theta}{\cos \theta_0} + \frac{Ce^{1-\sin \theta}}{\rho^b} \right],$$

where the constants are the same as those listed above. The corresponding F function is plotted in Figure 1 with $M = 4 \times 10^5$ (Smith, et al., 1974; 1975). Although this function exhibits better behavior near the magnetic axis, it is still unsatisfactory here. Replacing $Ce^{1-\sin \theta}/\rho^b$ by $-\log \cosh(1/\cos \theta_0)$ produces an f_1 which matches the b_μ data and is well behaved at $0°$, but insufficient southward field results because effects due to magnetopause currents have not been included in the model. Clearly an additional f function is needed, but infinite series techniques will likely be required.

Neglecting the presence of the magnetopause, the last closed field line crosses the magnetic equator at $\rho_c = 440$ for the preceding models. Under these conditions magnetic field lines originating at higher latitudes would not cross the equator and would therefore be considered as being open.

The Cylindrical Coordinate Model

Goertz, et al. (1974) have developed a model in cylindrical coordinates. For this case the axi-symmetric portion of the perturbation field is given by

$$B_1 = -\frac{1}{\rho} \frac{\partial f_1}{\partial z} \hat{\rho} + \frac{1}{\rho} \frac{\partial f_1}{\partial \rho} \hat{k}.$$

As before, a functional form for b_μ that is consistent with the current sheet data, etc., is
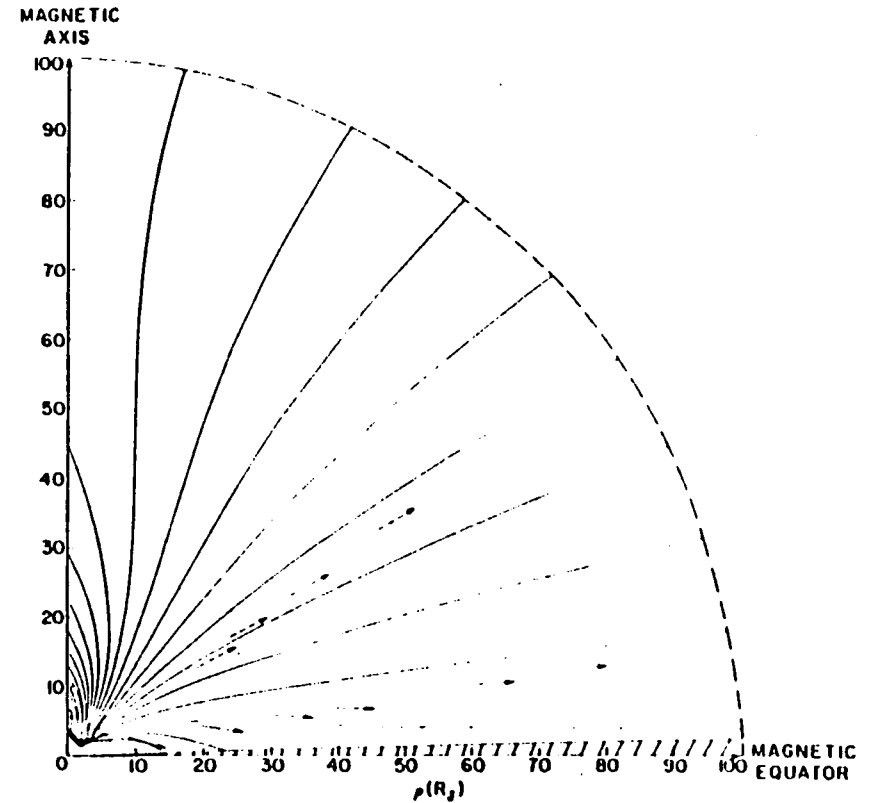
$$b_\mu = \frac{A}{\rho^a} \tanh z/D,$$

Figure 1. Meridional plane representation of the magnetospheric field as developed in a spherical coordinate representation. The solid and dashed arrows represent the average field direction measured at several points along the outbound trajectories of Pioneer 10 and 11, respectively. The shaded half angular width portion near the magnetic equator represents a portion of the equatorial current sheet configuration assumed in this model, and a first order approximation to the magnetopause boundary is also indicated. Regions over which the function is reliable are indicated in the text. The curves leave the $\rho = 2$ sphere at equally spaced angular intervals.

where the current sheet half-width, D, could be some function of ρ, i.e.,

$$D = D_0 \rho/\rho_0,$$

for a constant angular width sheet, or, in general,

$$D = D_0 (\rho/\rho_0)^b.$$

Since

$$b_\mu = -\frac{1}{\rho} \frac{\partial f_1}{\partial z}.$$

then

$$f_1 = - \frac{AD}{\rho^{a-1}} \log \cosh z/D + C(\rho).$$

The corresponding function for b_z is then

$$b_z = \frac{AD(a-1)}{\rho^{a+1}} \log \cosh z/D - \frac{bAz}{\rho^{a+1}} \tanh z/D + \frac{\partial C(\rho)}{\rho \partial \rho}.$$

Note that for $z/D \gtrsim 3$, $\log \cosh z/D$ is very nearly $z/D - \ln 2$, so that

$$b_z \bigg|_{z/D \ll 1} = \frac{AD}{\rho^{a+1}} (a - b - 1) \frac{z}{D} - \frac{AD(a-1)}{\rho^{a+2}} \ln 2 + \frac{\partial C(\rho)}{\rho \partial \rho}$$

Plotting b_ρ versus ρ for all $z/D \gtrsim 3$, and b_z versus ρ for fixed values of z/D, allows one to determine the constants in f_1. Goertz, et al. (1974) have plotted b_z in this manner and find

$$a + b + 1 = 2.77$$

$$C(\rho) = - \frac{15\,AD}{\rho^{a-1}}.$$

so that

$$f_1 = - \frac{AD}{\rho^{a-1}} (\log \cosh z/D + 15).$$

However, Goertz, et al. (1974) have plotted b_z versus ρ, where

$$b_z = b_\rho \sqrt{1 + b_\phi/b_\rho}$$

and

$$b_\phi = - k\rho b_\rho.$$

As a result, they obtain a power law representation of the component parallel to the magnetic equator which lies in the curved surface represented by

$$\phi + k\rho = \text{constant.}$$

However, the resulting f will be for such surfaces, does not represent an axi-symmetric field, and therefore cannot appropriately be added to the dipole f function, which is axi-symmetric. That is, the f functions to be added must share the same g function. Goertz, et al. (1974) found that

$$\frac{b_\phi}{\rho b_\rho} = - 8 \times 10^{-1}$$

and hence

$$b_s = b_\rho \sqrt{1 + (8 \times 10^{-3} \rho)^2}.$$

Since they found

$$b_s \propto \rho^{-1.67}$$

over the range $\rho = 20$ to $\rho = 80$, the corresponding ρ dependence for b_ρ should be corrected by the factor $\rho^{0.11}$, or

$$b_\rho \propto \rho^{-1.78},$$

so that

$$a = 1.78,$$

$$b = -0.01.$$

As a check on this, we determined the power law dependence of b_ρ on ρ directly and obtained values for a, A, and b of 1.75, 1.0×10^4, and $+0.02$ respectively for the range $\rho = 30$ to 80. Combining our results with those of Goertz, et al. (1974) we find that f_1 is given by

$$f_1 = - \frac{1.0 \times 10^4}{\rho^{0.75}} (\log \cosh z/D + 15) \qquad (30 \lesssim \rho \lesssim 80),$$

where b has been assumed equal to zero, and, based upon one well-defined current dip, D_0 has been set equal to 1 in units of Jovian radii. The total F function representing the axi-symmetric portion of the field is then

$$F = \frac{M\rho^2}{(\rho^2 + z^2)^{3/2}} - \frac{1.0 \times 10^4}{\rho^{0.75}} (\log \cosh z/D + 15).$$

A plot of F is shown in Figure 2. Applying the same conditions as for the spherical model, the above model predicts that the last closed field line will cross the magnetic equator at $\rho_c \cong 160$. Using $a = 15$ and $A = 7.5 \times 10^3$, Goertz, et al. (1974) obtain $\rho_c \cong 150$.

The Currents

The current configuration in the magnetosphere can be obtained simply from Ampere's law. Using the field expressions derived from the several f_1 functions one can obtain the configuration of the intense current sheet that exists at the magnetic equator as well as the volume currents. The ϕ components of the internal magnetospheric current system is found
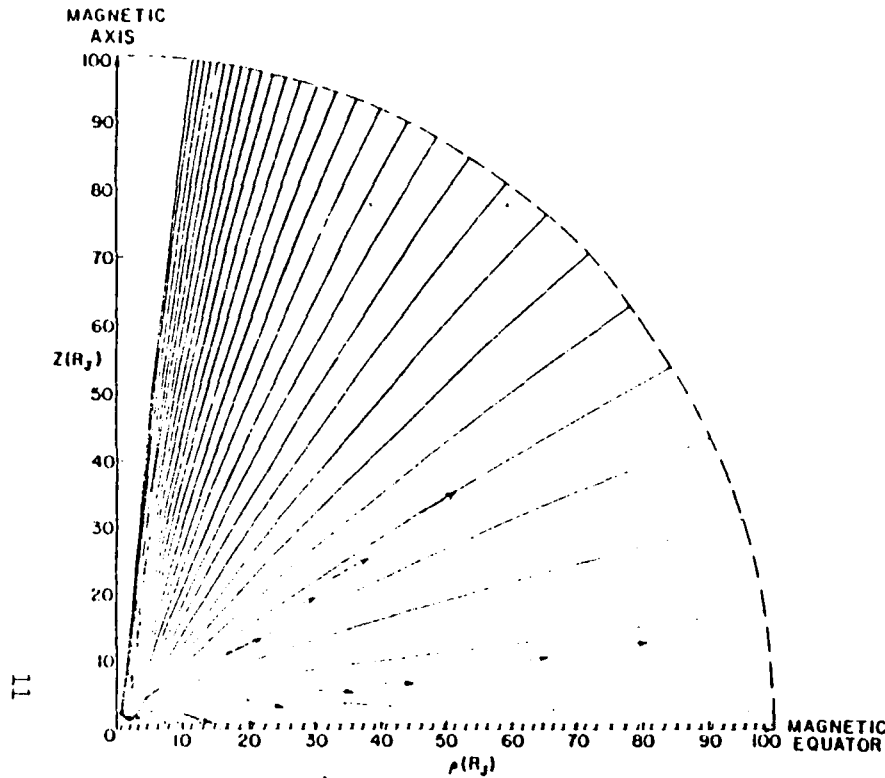
Figure 2. Meridional plane representation of the magnetospheric field as developed in a cylindrical coordinate representation. The solid and dashed arrows represent the average field direction measured at several points along the outbound trajectories of Pioneer 10 and 11 respectively. The shaded half width portion near the magnetic equator represents a portion of the equatorial current sheet configuration assumed in this model, and a first order approximation to the magnetopause boundary is also indicated. Regions over which the function is reliable are indicated in the text. The curves leave the $\rho = 2$ sphere at equally spaced angular intervals.

in each case to consist of a sheet current term plus a volume current term, where the sheet term for the spherical model is

$$J_\phi \bigg|_{sheet} = \frac{A \sin \theta}{\mu_0 R_J \rho^{t+1} \cos \theta_0} \, sech^2 \frac{\cos \theta}{\cos \theta_0}$$

and for the cylindrical model

$$J_\phi \bigg|_{sheet} = \frac{A}{\mu_0 R_J D \rho^a} \, sech^2 z/D.$$

Although the volume terms are negligible near the magnetic equator, they dominate near the magnetic polar axis. This is clearly an artifact of each model which will disappear when proper account of the magnetopause currents and of the inner cutoff radius of the current sheet or disc are included.

Mathematically terminating the field at the magnetopause allows one to solve for the magnetopause currents, and the corresponding boundary field direction can be determined for the several models and compared with the data. For example, a function, $t(\rho/\rho_0)$, which can terminate the field arbitrarily abruptly is

$$t(\rho/\rho_0) = \frac{1 + \tanh d(1 - \rho/\rho_0)}{2},$$

so that the terminated field, $\vec{B}'$, is given by

$$\vec{B}' = t(\rho/\rho_0)\vec{B}.$$

Here ρ_0 is the radial distance to the magnetopause (as a first approximation we assume the magnetopause boundary to be spherical) and d relates to the thickness of the boundary. In principle, B should be the total field. However, we still neglect the ϕ component of the perturbation field.

The above function terminates the preceding azimuthal currents at $\rho = \rho_0$ and in addition provides the magnetopause currents, i.e., for the spherical model

$$J_\phi \bigg|_{m.p.} = \frac{-d}{2\mu_0 R_J \rho_0} [sech^2 d(1 - \rho/\rho_0)] B_\phi$$

and for the cylindrical model (here $\rho = \sqrt{x^2 + y^2}$, normalized)

$$J_\phi \bigg|_{m.p.} = \frac{-d}{2\mu_0 R_J \rho_0} \left[sech^2 d \left(1 - \frac{\sqrt{\rho^2 + z^2}}{\rho_0} \right) \right] \left[\frac{zB_z - \rho B_z}{\sqrt{\rho^2 + z^2}} \right].$$

We find that B_ϕ for the spherical model is positive at all values of θ, so that the corresponding magnetopause current is clockwise, as viewed from the magnetic pole, at all latitudes. Hence, just prior to the magnetopause boundary the predicted field direction is southward, as is observed by both Pioneers 10 and 11 (Smith, et al., 1974; 1975). On the other hand, the bracketed term contained in the magnetopause expression for the cylindrical model becomes negative at magnetic latitudes greater than about 20°, so that the direction of the magnetopause current flow reverses from a clockwise direction at lower latitudes to a counterclock-

wise direction at higher latitudes. The corresponding field just inside the boundary is predicted to point *northward* at latitudes greater than 20° and southward at lower latitudes. Such a prediction appears to be in disagreement with the data, although it is interesting to note that prior to the outbound magnetopause crossings by Pioneer 11 there were intervals approaching 8 hours during which the magnetospheric fields pointed north of radial by roughly 20°. However, these are likely transient features related to a (possibly) northward component of the solar wind flow velocity.

Discussion

Since the functions plotted in Figures 1 and 2 were derived from the Pioneer 10 outbound data, they were developed from data taken within about 20° of the magnetic equator and over the radial range $20 \lesssim \rho \lesssim 80$, and qualitatively represent the magnetospheric field configuration in meridional planes that lie near the dawn terminator. However, one notes that the models also qualitatively fit the Pioneer 11 data quite well, which extends the latitude range of the functions to perhaps 40° (the Pioneer 11 inbound data is qualitatively very similar to the Pioneer 10 outbound data) and to about 40° sunward of the dawn meridian. As is evident from the figures, both models should be considered unreliable at latitudes greater than about 45°.

A basic difference between the two models is the fact that one is for a constant angular width current sheet (the spherical coordinate model, Figure 1) while the other is for a constant thickness current sheet (the cylindrical coordinate model, Figure 2). Likely the actual case lies somewhere between these two current sheet configurations. Both permit the current sheet to exist to the center of the planet, although it must be cut off at some inner radius $\rho \gtrsim 2$, since one would not expect the sheet to exist within the centrifugal-gravitational balance distance of several radii.

Another basic difference involves the direction of flow of the magnetopause currents and the corresponding direction of the magnetopause field. Predictions based upon the spherical model are more consistent with the measurements.

There are also a number of factors regarding the constants derived for the models that should be mentioned. For example, in the case of the cylindrical coordinate model, the value of c in f_1 is determined from h_z versus ρ at constant z/D, but this requires a knowledge of D. The evaluation of the constants a, A, and h depends critically upon the accurate determination of the actual power law dependence of D on ρ. The current sheet half-width is one of the most uncertain parameters, and its

dependence upon ρ is particularly difficult to determine directly from the plots of B versus ρ. The constants contained in the expression for f_1 are self-consistent, and the model appears to establish the ρ independence of D. Similar comments can be made regarding the constant angular width model as well. Unfortunately, a brief study of the variation of the widths of the field dips has not shed much light on this crucial point, except that the data tend to favor the constant angular width model.

In the study by Goertz, et al. (1974), the determination of a and D (their b_0) from a plot of b_r instead of b_ρ causes the resulting function that is to represent the shape of the field in meridional planes to be a mixture of f functions requiring different g functions. On the other hand, in our determination of these constants for the cylindrical model, we have used only f functions that have the same g function. Because the spiraling of the field was not excessive, the disagreement with the results of Goertz, et al. (1974) is not great, and a comparison of the plots of the field lines shows them to be quite similar.

Any interpretation regarding the value of ρ_c (where $B_L = 0$) that is derived from the models should be viewed with caution since the model fits the data only out to about 80 or 85 R_J, and hence these cutoff radii should be considered as possible artifacts of the models. An artifact of this kind is meaningless because the magnetopause currents have been neglected in the derivation of the f functions. As noted earlier, it is tempting to assume that field lines leaving the planet at higher magnetic latitudes than those related to ρ_c are open field lines and that they merge with the interplanetary field. But the data show that the field lines are southward at the magnetopause, suggesting that they are closed by the magnetopause currents. In the sense of field lines and particle trapping, these lines clearly will not have trapped particles on them. The last closed field line which could contain trapped particles should be the one which crosses the equator just prior to the magnetopause boundary.

The particles in the intense equatorial current sheet likely result from plasma flow due to the combined action of a Jovian "polar wind," much like that postulated for Earth (Banks and Holzer, 1969), plus the strong centrifugal force caused by the large size and rapid rotation of the magnetosphere. The balance of pressures at the magnetopause likely must include that exerted by a radial flow of polar wind ions moving parallel to the essentially radial field lines in the magnetosphere. Perhaps such a plasma flow also provides a significant stabilizing influence for the large-scale magnetosphere configuration reported here, since one would otherwise expect the solar wind to blow the high latitude field lines back into the tail because of the relatively weak magnetic pressure exerted at the magnetopause (Smith, et al., 1974). A study of the Pioneer

11 outbound data will provide some important information in this regard, although much higher latitude data are clearly needed.

Further studies of the magnetosphere will likely require the use of perturbation techniques (Stern, 1967) in order to obtain more well-behaved functions at high latitudes and to allow for a nonspherical magnetopause boundary. Other studies being conducted at the present time will merge models developed for the range $1 \leqq \rho \leqq 6$ with the magnetospheric models reported here. In this regard, magnetospheric studies establish reasonable estimates of the magnetospheric current systems and detailed attempts at merging the two programs will establish, among other things, the inner cutoff radius of the current sheet.

This research was supported in part by the National Aeronautics and Space Administration under NASA-Ames contract NAS2-7358.

List of References

Banks, P. M., and T. E. Holzer. High latitude plasma transport: the polar wind. *J. Geophys. Res.* 74, 6317, 1969.

Bird, M. K. Solar wind access to the plasma sheet along the flank of the magnetotail. *Planet. Space Science* 23, 27, 1975.

Euler, L. Sectio secunda de principiis motus fluidorum, *Novi Comentarii Acad. Sci. Petrolotance*, 14, 270, 1769; reprinted in Leonhardi Euleri Opera Omnia, series II, vol. 13, p. 73, Swiss Society for Natural Sciences, 1955.

Goertz, C. K., B. A. Randall, and M. F. Thomsen. A model for the Jovian magnetic field. Paper presented at the fall 1974 meeting of the American Geophysical Union, Dec. 12-17, 1974.

Jones, D. E., E. J. Smith, L. Davis, Jr., P. J. Coleman, Jr., D. S. Colburn, P. Dyal, and C. P. Sonett. Pioneer 11 measurements of Jupiter's magnetic field. Paper presented at the spring 1975 meeting of the Utah Academy of Sciences, Arts, and Letters, March 28, 1975 (abstract this issue of the Proceedings).

Mihalov, J. D., H. R. Collard, D. D. McKibbin, J. H. Wolfe, and D. S. Intriligator. Preliminary Pioneer 11 encounter results from the Ames Research Center plasma analyzer experiment. To be published in *Science*, 1975.

O'Brien, V. Axi-symmetric magnetic fields and related problems. *J. Franklin Institute* 275, 24, 1963.

Smith, E. J., L. Davis, Jr., D. E. Jones, P. J. Coleman, Jr., D. S. Colburn, P. Dyal, C. P. Sonett, and A. M. A. Frandsen. The planetary magnetic field and magnetosphere of Jupiter: Pioneer 10. *J. Geophys. Res.* 79, 3501, 1974.

Smith, E. J., L. Davis, Jr., D. E. Jones, P. J. Coleman, Jr., D. S. Colburn, P. Dyal, C. P. Sonett. Jupiter's magnetic field, magnetosphere and interaction with the solar wind. To be published in *Science*, 1975.

Stern, D. P. The motion of magnetic field lines. *Space Science Rev.* 6, 147, 1966.

Stern, D. Geomagnetic Euler Potentials. *J. Geophys. Res.* 72, 3995, 1967.

Truesdell, C. The kinematics of vorticity, Indiana University Press, 1954.

1. Report No. NASA CR-166366	2. Government Accession No.	3. Recipient's Catalog No.
4. Title and Subtitle Pioneer 10/11 Data Analysis of the Magnetic Field Experiment		5. Report Date June, 1982
		6. Performing Organization Code
7. Author(s) Douglas E. Jones		8. Performing Organization Report No.
9. Performing Organization Name and Address Brigham Young University Provo, Utah		10. Work Unit No.
		11. Contract or Grant No. NAS2-7358
12. Sponsoring Agency Name and Address National Aeronautics and Space Administration Washington, DC 20546		13. Type of Report and Period Covered Contractor - Final Report
		14. Sponsoring Agency Code

15. Supplementary Notes
Technical Monitor: Christopher A. Liedich, M/S 244-8, NASA Ames Research Center, Moffett Field, CA 94035 (415) 965-5692 FTS 448-5692

16. Abstract
This final report covers work conducted by Brigham Young University personnel in support of the Pioneer missions to Jupiter (10, 11), and Saturn (11) as well as the reduction, analysis and interpretation of magnetic field data obtained by the vector helium magnetometer (VHM) on the Pioneer 10 and 11 spacecraft. Initially, efforts were concentrated primarily on the interplanetary data, and those aspects of the data of relevance to obtaining a better understanding of the interaction of the magnetized solar wind with the terrestrial magnetic field. However, after encounters of Jupiter and Saturn, the emphasis of research was directed primarily to an analysis of the planetary data. In particular, it soon became clear that there was a need for modelling of the various candidate magnetospheric currents suggested by the data. Over the period of this contract (7/1/73-12/31/81) BYU has supported the launch, cruise, and encounter phases of the Pioneer 10 and 11 missions, published 16 papers, presented 15 papers, and had 19 abstracts of papers published. A listing of the papers and abstracts published is given in the "List of Publications." The following sections summarize the work conducted in various research areas conducted under this contract. Included are results not published as yet, but which are planned to be published.

17. Key Words (Suggested by Author(s)) Pioneer 10 and 11 Planetary magnetospheres Interplanetary magnetic fields	18. Distribution Statement Unclassified - Unlimited SUBJECT Category - 91		
19. Security Classif. (of this report) Unclassified	20. Security Classif. (of this page) Unclassified	21. No. of Pages 80	22. Price*

End of Document